LEVERAGING PROCESSOR ELECTROMAGNETIC RADIATION FOR RADIO TOMOGRAPHY

W.M.O.E. WICKRAMASINGHE

2025

Leveraging Processor Electromagnetic Radiation for Radio Tomography

W.M.O.E. Wickramasinghe
Index No: 20002149

Supervisor: Chamath I. Keppetiyagama
Co-Supervisor: Asanka P. Sayakkara

May 2025

Submitted in partial fulfillment of the requirements of the
B.Sc (Honours) in Computer Science Final Year Project

Declaration

I certify that this dissertation does not incorporate, without acknowledgment, any material previously submitted for a degree or diploma in any university and to the best of my knowledge and belief, it does not contain any material previously published or written by another person or myself except where due reference is made in the text. I also hereby give consent for my dissertation, if accepted, to be made available for photocopying and for interlibrary loans, and for the title and abstract to be made available to outside organizations.

Candidate Name : W.M.O.E. Wickramasinghe

.....

Signature of Candidate Date: 2025/06/29

This is to certify that this dissertation is based on the work of Ms. W.M.O.E. Wickramasinghe under my supervision. The thesis has been prepared according to the format stipulated and is of acceptable standard.

Principle Supervisor's Name : Dr. Chamath I. Keppetiyagama

.....

Signature of Supervisor Date: 30--6-25

Co-Supervisor's Name : Dr. Asanka P. Sayakkara

.....

Signature of Supervisor Date: 2025-06-29

Abstract

Radio Tomographic Imaging (RTI) is a promising technique for imaging non line of sight areas, but current implementations require complex setups with multiple, symmetrically placed transceivers and costly, dedicated radio circuits. These systems are difficult to be used in embedded and IoT applications and are highly sensitive to variations in terrain and surface structure, which can significantly impact signal measurements.

This research investigates an approach that leverages unintentional Electromagnetic (EM) radiation emitted by processors within computing devices. The results demonstrate that an object in Line of Sight (LOS) between the signal source and receiver causes measurable variations in the received signal from 0.65 to 3.52 dBm. But this value highly depends on the area of interest and surrounding. According to the results, changes are detectable up to 2.4 m from the signal source in a cluttered indoor environment and up to 3 m in an open outdoor environment. Moreover, using signal propagation characteristics of a single link, the location of an object in the LOS can be estimated up to 0.1072 m mean absolute error with two possible locations which can be reduced to one correct estimation with particle filters like Kalman filter.

To date, most efforts in the RTI field have focused on developing algorithms that enhance tomographic image accuracy. However, there is a noticeable gap in work addressing computational efficiency and practical feasibility. Building on the observed characteristics of unintentional EM radiation from the signal source, this research proposes a novel weight model algorithm designed to reduce computational cost compared to the statistical tomographic imaging model introduced by Wilson and Patwari in “Radio Tomographic Imaging with Wireless Networks”.

Acknowledgment

This research would not have been possible without the support and encouragement of many individuals.

I am deeply grateful to Dr. Chamath Keppetiyagama and Dr. Asanka Sayakkara for their invaluable guidance, insightful suggestions, and continuous support throughout every stage of this work as supervisors. I am also sincerely thankful to Dr. Kasun Karunanayake for his thoughtful advice, especially during times of uncertainty and conflict.

I am much grateful for the opportunity to engage in insightful discussions with Prof. Thiemo Voigt regarding the results of this research. His input has been immensely helpful in giving them greater meaning.

I also extend my thanks to my colleagues and friends who assisted in data collection, as well as to the academic and ground staff at UCSC for providing the essential facilities and a supportive environment.

A special note of gratitude goes to my seniors, Nethmi Rodrigo and Lasith Niroshan, for their generous guidance and for always being willing to share their knowledge, especially during challenging moments in this journey.

Table of Contents

List of Figures

List of Tables

List of Acronyms

RTI Radio Tomographic Imaging

AoI Area of Interest

RF Radio Frequency

CT Computed Tomography

MRI Magnetic Resonance Imaging

OCT Optical Coherence Tomography

AOA Angle of Arrival

AOD Angle of Departure

TOF Time of Flight

DFS Doppler Frequency Shift

RSSI Received Signal Strength Indicator

CSI Channel State Information

RSS Received Signal Strength

CIR Channel Impulse Ratio

NLOS Non-Line-of-Sight

LOS Line of Sight

UWB Ultra Wideband

IoT Internet of Things

EM Electromagnetic

DVFS Dynamic Voltage and Frequency Scaling

ML Machine Learning

FFT Fast Fourier Transformation

STFT Short Time Fourier Transformation

WT Wavelet Transformation

PSD Power Spectral Density

CPU Central Processing Unit

SNR Sound to Noise Ratio

SDR Software Defined Radio

PSU Power Supply Unit

IQ In-phase and Quadrature

TSVD Truncated Singular Value Decomposition

FTD Foreground Target Detection

Chapter 1

Introduction

Humans have evolved from taking data from natural sensors to taking more detailed and processed data using advanced techniques. One aspect that has been surpassed by developments in technology is observing objects and phenomena that are located Non-Line-of-Sight (NLOS) using tomographic imaging techniques.

Tomography is the technique of producing images by analyzing cross sectional images; i.e., projections. Cross sectional images are generated by gathering data from different angles using reflections or transmissions. This is an emerging technology of computer vision, finding new approaches and uses. Another significant feature in tomographic imaging is the possibility of using it as a wireless sensing method. As the medium of data for input of tomography, the spectrum of EM waves, such as X-rays, radio waves, or WiFi signals, are used.

A sensor network consist of many transmitters and receivers, producing wireless links that connects each node to every other node. In a sensor network implemented as in Figure 1.1, the transmitter emits wireless signals which propagate through air and are detected by the receiver. During the propagation, signals are affected by reflection, diffraction, refraction, shadowing or scattering which causes strength, amplitude, or phase changes due to mobile or stationary objects in the environment. Therefore, obstructions along the propagation path can be identified according to deviations of the received signal from the base signal (Yang et al. 2021, Wilson & Patwari 2011). A

tomographic image is constructed by analyzing variations in the link quality parameters of multiple links deployed across a given area. Thus the basic requirement is to be able to detect an object in the free path of a single link.

Localization with RTI provide position information of an observed object in a target area and requires a setup of multiple links covering an area and frameworks like Kalman filter to find location coordinates of a moving object (Wilson & Patwari 2011).

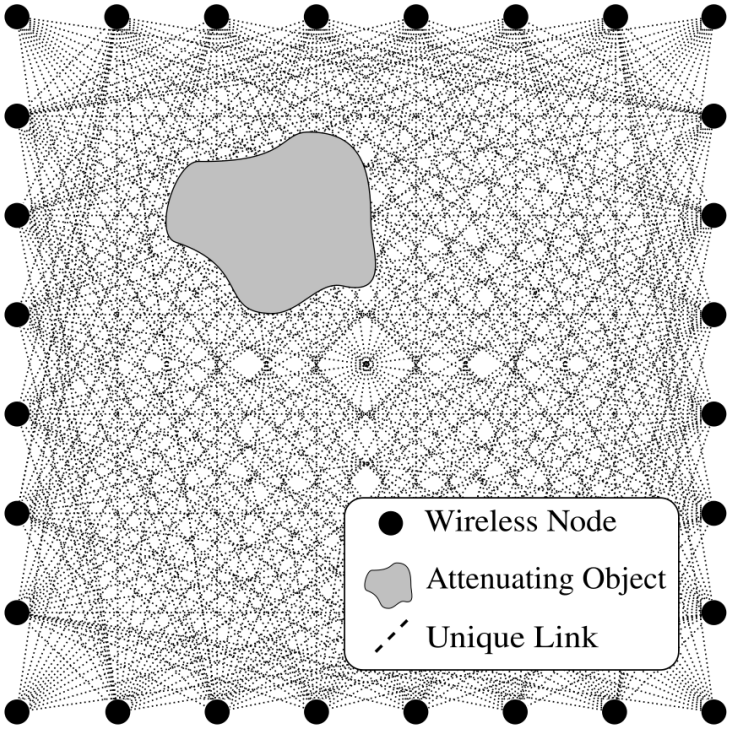

Figure 1.1: Common RTI setup (Adapted from (Wilson & Patwari 2010))

All the methods that have been developed so far for Radio Frequency (RF) tomography are not feasible in situations where an intentional EM wave source is not present or can not be placed. Hence, this research study the feasibility of using unintentional EM radiations emitted by processors of computing devices as the RF signal source. These are generated due to changing currents inside the physical system caused by switching of transistors or the flow of current through circuits (Mulder 2010) .

Through a series of controlled experiments, this research demonstrates that when an object obstructs the LOS between such a signal source and a receiver, it results in detectable changes in RSS ranging from 0.65 to 3.52 dBm. The disturbances are

measurable up to a distance of 2.4 m in cluttered indoor settings and up to 3 m in open outdoor environments. Additionally, by analyzing the signal characteristics of a single transmission link, the object's position within the LOS can be estimated with a mean absolute error of approximately 0.1072 m. While this estimate initially yields two potential locations, the ambiguity can be resolved using particle filters such as the Kalman filter.

While prior work in RF tomography has largely prioritized enhancing image accuracy, there has been relatively little focus on computational efficiency and real-world practicality. To address this, this study introduces an improved weight model that leverages the nature of unintentional EM radiation to reduce the computational overhead.

1.1 Motivation and Background

Tomography finds applications in medical, construction, defense and military, elderly care, and in Internet of Things (IoT). Among them, applying tomography in localization, tracking and crowd counting in enclosed or unreachable spaces are significant as a non intrusive and privacy-preserving solution.

Optical sensing methods including cameras and active sensing methods involving a tracking device are less effective in situations such as rescue missions where victims are trapped and in battlefields where direct access is not possible in comparison to wireless sensing. In contrast, wireless sensing methods can operate in NLOS, with less visibility, smoke or fog. But wireless sensing methods implemented with millimeter Wave, RF, Bluetooth, or Ultra Wideband (UWB) require signal sources intentionally deployed around the enclosed area.

Despite the advantages, setting up the wireless sensor network can be challenging and time consuming, especially in time critical situations where lives are at risk. Furthermore, the accuracy of the sensor network will depend on the surface variations. And another human will have to take the risk of implementing the setup even in critical situations.

Hence it is necessary to minimize the setup effort and reduce errors based on the

surface and the environment. A promising solution will be using unintentional EM radiations of computing devices to create the tomographic image. This approach is highly feasible in homes, offices, and other spaces where computing devices are commonly used.

Furthermore, transceivers used in IoT applications typically require significant power and resources to generate signals of the communicating frequency. However, leveraging unintentional EM radiation can reduce setup costs, as well as power and resource consumption.

1.2 Research Gap

The significance of RTI is due to its passive, wireless and non intrusive characteristics with the ability to operate in NLOS. A basic RTI setup requires a series of transceivers to be implemented around the enclosed area to be monitored.

However, this setup has significant limitations. Transceivers should be placed at a constant height. The arrangement must be symmetric, regular, and static while operating. Also, failure of one node will have a significant effect on the voxel grid. Additionally, placing nodes and supplying power to nodes require considerable effort, resources and time. Moreover, continuously operating the radio chip is costly in a low power system. Therefore, the main drawback identified in RTI is the reliance on purpose-built transmitters as the medium of data.

These limitations can be addressed by using existing RF sources as the source of medium. Unintentional EM radiations, generated by active computing devices like laptops and smartphones, offer a valuable alternative.

1.3 Research Question

- What is the accuracy of tomography when utilizing unintentional EM radiation from computers?

  Hypothesis: When EM waves propagate, signals are affected by reflection, diffraction, refraction, shadowing or scattering which causes strength, amplitude, or phase changes due to objects in the path.

1.4 Aim and Objectives

Project Aim

This project aims to find a solution to the problem of the absence of an intentional RF signal source in the tomography setup by studying the feasibility of localization using unintentional EM radiations generated by processors of computing devices as a side channel.

Objectives

1. Identifying the range or frequency of EM radiation from the target device.
2. Observe the sensitivity of unintentional EM radiations generated by computing devices processors to changes caused by surrounding obstructions, noise interferences.
3. Determine the maximum range at which the system can detect deviations caused by objects.
4. Develop a model to estimate the location of an object placed on the signal link.

1.5 Scope and Assumptions

In Scope

- A single, pre-selected device will be used as the source of unintentional EM radiation.
- The study is limited to a single signal link established in LOS and a single link quality parameter (RSS).
- A model will be developed to evaluate the feasibility of object localization.
- Although RSS is known to vary with CPU workload, this research maintains a constant workload throughout the experiments.

Out of Scope

- The statistical model will not explore applications beyond object localization.
- This research does not consider the study of NLOS signals due to the high variability introduced by different obstacle materials, thicknesses, and propagation environments.
- Remote identification of signal sources using EM radiation is excluded, as this has already been addressed in prior research.
- The study will not investigate or compare different types of EM radiation sources (Computing devices).
- Signal amplifiers, directional antennas, or other signal enhancement tools will not be used in the experimental setup.

Assumptions

- A link with only one obstruction is assumed at all aspects.

Chapter 2

Literature Review

Sensor networks with wired devices require a vast number of devices to be interconnected. Deploying and maintaining such a wired sensor network is costly and the network becomes complex as the scale increases. In contrast, wireless sensor systems are more feasible since physical space is already flooded with wireless signals that are used for illumination and communication. Applications of wireless sensing are already in use within smart homes, security, and biometrics recognition. The key feature of a wireless, passive sensor network is that the observed targets do not need to have a tracking device. Hence it bears the characteristics of being wireless, sensor less and contactless (Yang et al. 2021).

Video camera systems are a prominent example of wireless passive sensor networks but contain several concerns. They require sufficient illumination conditions and the environment to be opaque but still capture only objects in the LOS. The use of video cameras has raised privacy concerns in various contexts and can be considered as invasive. Also, video cameras are unable to serve their purpose in situations with smoggy air such as a fire, polluted city, mist or battlefields with restricted direct access (Bocca et al. 2013).

RTI is a type of tomography that uses RF signals to create a map of the observed space. Tomography refers to the technique of producing 2D or 3D images by analyzing cross sectional images and its applications are implemented using diverse mediums. RTI

systems using RF signals have better features concerning privacy of the users in the area and the ability to track and localize objects even through walls compared to video camera systems. They are minimally invasive compared to other wireless sensor networks and are cheaper (Bocca et al. 2013, Kabir et al. 2022).

2.1 Sensing Mediums for Tomography

Optical Coherence Tomography (OCT), Ultrasound scanning, Magnetic Resonance Imaging (MRI), and Computed Tomography (CT) are examples of tomography used in the medical field. OCT produces high resolution cross sectional images of tissues using near infrared waves. MRI images soft tissues such as the brain or heart using a strong magnetic field and radio waves. Using X-rays, CT can create cross sections of a human body as images.

WiFi tomography is another subdomain of RTI. While RTI uses RF waves, WiFi tomography uses frequencies in the 2.4 GHz and 5 GHz bandwidth (Kabir et al. 2022).

Each medium used to collect data has characteristics that makes it suitable for a specific task and limitations that would restrict performance. A comparison of data collecting mediums, characteristics and restrictions are in Table 2.1.

Medium	**Characteristics**	**Limitations**
Near-infrared waves	High resolution, suitable for imaging tissues	Limited depth penetration, high cost
Sound waves	Non-invasive, good for soft tissues	Lower resolution, limited penetration in dense tissues
Strong magnetic field and radio waves	High contrast images of soft tissues, no ionizing radiation	Expensive, long scan times, not suitable for patients with metal implants
X-rays	Detailed cross sectional images, fast imaging	Ionizing radiation exposure, high cost
WiFi	Non invasive, uses existing WiFi infrastructure	Limited resolution, vulnerable to interference

Table 2.1: Comparison of Medium, Characteristics, and Limitations

Wireless sensing systems are implemented using various technologies but among them, RF tomography stands out due to collective attributes in performance, adaptability,

scalability, and ability of omni-directional penetrations through obstacles.

2.2 Link Quality Parameters

WiFi tomography considers link quality measurements generated by the transmitted signal. A transmitted WiFi signal consists of subcarriers at a granular level.

In wireless sensing, the target is independent of the environment but it is highly interdependent in the measured values of a signal. As a result, various parameters can be estimated to analyze the received signals and detect causes of variations made in the link. These parameters are calculated from link quality measurements like the Received Signal Strength Indicator (RSSI) and Channel State Information (CSI). RSSI is a representation of the strength of the phasor sum of multi paths. CSI provides details about the phase and the amplitude of subcarriers. The observed received signal is the phasor sum of every signal that reaches the receiver from different paths. Some other link quality parameters are (Yang et al. 2021),

- Time of Flight (TOF) - TOF represents the duration a signal takes to propagate from the transmitter to the paired receiver. Changes in the TOF will introduce phase shifts to the signal. Channel Impulse Ratio (CIR) depicts TOF of all the paths.

- Angle of Arrival (AOA) - AOA represents, from which direction the signal has reached the transmitter.

- Angle of Departure (AOD) - AOD stands for the direction in which the transmitted signal travels to reach the receiver.

* Both AOA and AOD are used to find the local coordinates of nodes in a wireless sensor network

- Doppler Frequency Shift (DFS) - DFS is introduced by moving objects in the propagation path or relative movements of the nodes or both. Human body motions

can be identified using this as DFS depends on the location and velocity of the observed target.

Effect of a person on a signal link varies based on signal frequency being used, transmitting power, and environment. A comparison of effect of a person on a LOS link is as follows (Table. 2.2),

Ref.	**Type of Study**	**Wireless Technology**	**Test Field**	**Major Findings**
Alshami et al. (2015)	Experiment	WLAN, 2.4 GHz radio devices	Indoor	Human movement decreased the RSSI by 2 to 5 dBm; this could lead to a distance error exceeding 2 m
Liu et al. (2016)	Experiment	MicaZ nodes, CC2420, 2.4 GHz ZigBee/IEEE 802.15.4	Indoor	Human movement across LoS reduced RSSI by 5 to 10 dBm, depending on distance between transmitter and receiver
Kaltiokallio, Yigitler & Jantti (2014)	Experiment	CC2431, 2.4 GHz ZigBee/IEEE 802.15.4	Indoor	Human movement across LoS caused RSSI variation, influenced by link distance
Sasiwat et al. (2019)	Experiment	CC2420, 2.4 GHz ZigBee/IEEE 802.15.4	Indoor	RSSI varied with person's predefined positions across LoS; center position caused RSSI to drop 8 dBm; bi-directional links showed same pattern

Table 2.2: Summary of Experimental Studies on Human Movement and RSSI Variations (Adapted from Wounchoum et al. (2022))

2.3 Methods

There are two widely used approaches for RTI.

- Fingerprint-based method
- Model-based method

Fingerprint-based method has a pre trained database of data labeled with position and when in use measurements are compared with those in database to estimate position. This method is more accurate but training phase is time and resource consuming and require much effort to collect data. Moreover, the process has to be repeated when changing the environment.

Model-based method is based on a semi empirical weight model. This method is computationally efficient but the dynamic and sensitive nature of RSS introduces noise and pseudo targets in the tomographic image (Ke et al. 2019). Over the years different methods have been proposed to quantify the change in RSS in a link due to an obstruction (Shukri & Kamarudin 2017, Bocca et al. 2013).

The initially introduced RTI method is shadowing-based RTI. This method correlates the shadowing effect caused by the human body on the RSS with the position of an individual (Dharmadasa et al. 2018, Shukri & Kamarudin 2017).

The attenuation-based method takes into consideration an RSS value at a specific time and the base RSS value. The base RSS value is the average RSS measured during the calibration period. Generally, the difference between the two values would suggest an obstruction (Bocca et al. 2013, Wilson & Patwari 2010).

Histogram-based RTI considers two histograms. RSS values gathered during the calibration period are represented in the long term histogram and the short term histogram is based on the recent RSS values. The kernel distance between two histograms depicts a change in RSS value which is mostly caused by an obstruction (Bocca et al. 2013).

Histogram and Attenuation-based RTI methods are used to detect both stationary and nonstationary objects but both require an initial calibration period without obstructions

in the link (Bocca et al. 2013).

Variance-based RTI measures the RSS variance caused by mobile objects in the Area of Interest (AoI) within two consecutive time periods (Wilson & Patwari 2011).

2.4 Inverse Problem

The inverse problem is the core of tomography. In the context of RTI, results are the values collected from receivers regarding the signal transmitted. An inverse problem would be to derive attenuation coefficients or distribution of materials. Obtained values can provide further details about the path that the signal propagated through (Tarantola 2005) .

The inverse problem we come across in RTI is mostly ill-posed since measurements obtained are noisy, indirect, incomplete and may produce multiple solutions. The ill-posed nature of an inverse problem results in meaningless outputs by amplifying even small noises significantly (Wilson & Patwari 2010, Tarantola 2005).

2.5 Setup

A basic setup of the RTI system to obtain link quality measurements is as follows,

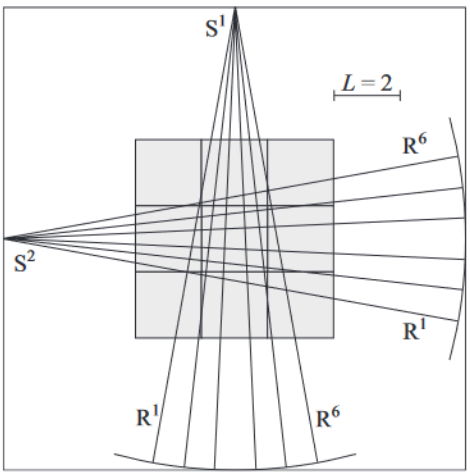

Figure 2.1: Simple setup to obtain RTI measurements (Adapted from (Tarantola 2005))

In Figure 2.1, S^1 and S^2 are transmitters. $R^1, ...R^6$ are receivers. R_{ij} is the link

between source i and receiver j. The AoI is assumed to have nine homogeneous portions known as voxels in RTI (Tarantola 2005).

Priori information required is the vector of integrated attenuation and the vector of linear attenuation coefficients (Tarantola 2005).

A linear attenuation coefficient represents a measurement of deviation in the link quality attribute from the expected value. For the above example scenario, the vector will take the following shape (Tarantola 2005),

$$A = \begin{pmatrix} a_{11} & a_{12} & a_{13} \\ a_{21} & a_{22} & a_{23} \\ a_{31} & a_{32} & a_{33} \end{pmatrix}$$

Integrated attenuation is a measure of path loss. For the above example scenario the vector will take the following shape (Tarantola 2005).

$$L = \begin{pmatrix} l_{11} & l_{12} & l_{13} & l_{14} & l_{15} & l_{16} \\ l_{21} & l_{22} & l_{23} & l_{24} & l_{25} & l_{26} \end{pmatrix}$$

By using a vector of integrated attenuations, a better estimation of linear attenuation coefficients without noise and uncertainty is obtained in the inverse problem. The process involves least squares theory to reduce noise and improve accuracy (Wilson & Patwari 2010, Tarantola 2005).

This being the basis of RTI, the exact mathematical model used is decided by the specific application and actual experimental setup.

2.6 Regularization

Due to the ill posed inverse nature of the problem, regularization techniques are being used to increase the accuracy by reducing noise, smoothing and enhancing edges.

Some algorithms in use are briefly mentioned below.

Tikhonov regularization

The Tikhonov Regularization can be described as follows (Niroshan et al. 2018),

$$f(x) = 1/2\|Wx - y\|^2 + \alpha\|Qx\|^2 \tag{2.1}$$

W : The weight matrix. It models how the actual signal/image is projected into measurements.

y: The measured data or observations.

Q: The Tikhonov matrix. This is used to enforce smoothness or apply prior knowledge.

α: Regularization parameter.

x_{TIK} is the reconstructed signal or image that best explains the measurements y, while also being smooth or regular than the input.

$$x_{\text{TIK}} = (W^T W + \alpha Q^T Q)^{-1} W^T y \tag{2.2}$$

If we define

$$P_{\text{TIK}} = (W^T W + \alpha Q^T Q)^{-1} W^T \tag{2.3}$$

then the Tikhonov solution can be expressed as:

$$x_{\text{TIK}} = P_{\text{TIK}} \cdot y \tag{2.4}$$

P_{TIK} is a matrix that maps y directly to x_{TIK}, and it can be precomputed to make reconstruction very fast for different y values.

Truncated Singular Value Decomposition

By discarding small singular values, Truncated Singular Value Decomposition (TSVD) prevents the solution from being corrupted by noise. It acts as a low-pass filter in the information space.

TSVD is achieved by removing small singular values from the transfer matrix W (Niroshan et al. 2018).

$$x_{\text{TSVD}} = \sum_{i=1}^{k<N} \frac{1}{\sigma_i} \mathbf{v}_i^T \mathbf{y}\, \mathbf{u}_i \tag{2.5}$$

x_{TSVD} : The reconstructed or estimated image using the TSVD method.

y: The measured data

v_i: The i^{th} right singular vector of the system matrix W.

u_i: The i^{th} left singular vector of matrix W.

σ_i: The i^{th} singular value. It scales the contribution of each singular vector pair.

k: The truncation threshold, indicating how many of the largest singular values and associated vectors are retained. $k < N$, where N is the total number of singular values.

Total Variation

Total variation regularization is used in image reconstruction to enhance image quality by promoting sharp edges while suppressing noise. (Niroshan et al. 2018):

$$f(x) = \frac{1}{2}\|Wx - y\|_2^2 + \alpha\, \text{TV}(x) \tag{2.6}$$

where the total variation term is given by:

$$\text{TV}(x) = \sum_i |\nabla x|_i \tag{2.7}$$

Here, $|\nabla x|_i$ denotes the i-th element of the gradient of x.

Total variation regularization minimizes the total amount of variation across the image by adding a penalty term to the reconstruction objective that is proportional to the sum of the absolute gradients, which helps reduce noise without blurring important features.

Regularization techniques are applied on y before constructing the tomographic image. In contrast, there are other methods that perform the same purpose after constructing the image. Foreground Target Detection (FTD) is an example (Ke et al. 2019). It is applied on pixels. First, pixels are divided considering a threshold value based

on average brightness value of all pixels. This results in two categories as background and foreground pixels. Then The value of background pixels are set to 0, eliminating their effect.

2.7 Weight Model

Accuracy of an RTI method depends mostly on the weight model. It represent the relationship between the shadowing effect of an object on the RF link and the location of the object (Ke et al. 2019).

Weight model differ in the way they perform the weight function considering the area of the link, fade level along the link and variation of the object on the link based on its position.

Line model, Ellipse model and Gaussian model consider the area of the link to assign values to the weight model.

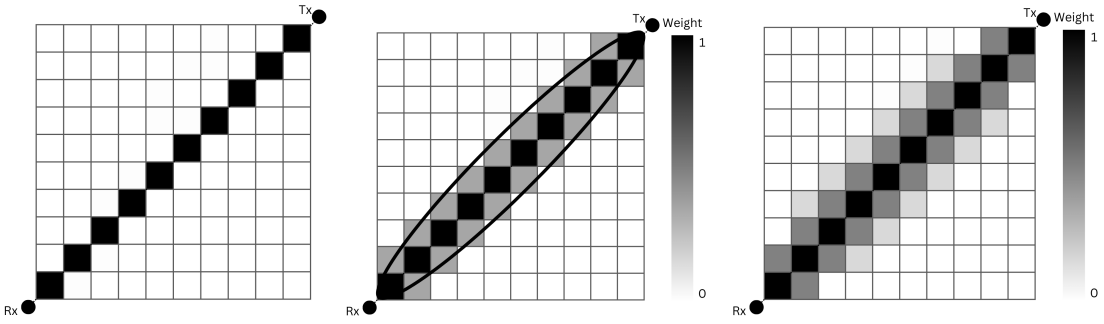

(a) (b) (c)

Figure 2.2: Weight models (a) Line model (b) Ellipse model (c) Gaussian model

Line Model

Line model assumes that the RSS of a wireless link is primarily affected by the presence of objects located along the LOS path between a transmitter and a receiver as shown in Figure 2.2a. To calculate the weights, it uses the Eq. 2.8 (Niroshan et al. 2018):

$$W_{l,i} = \begin{cases} 1, & \text{if link } l \text{ intersects voxel } i \\ 0, & \text{otherwise} \end{cases} \tag{2.8}$$

Ellipse Model

Unlike the line model, which assumes signal attenuation only along the direct LOS path, the ellipse model considers a broader region between the transmitter and receiver. Specifically, it defines an ellipse with the transmitter and receiver at its foci and includes all voxels whose total distance to the two endpoints is less than a specified threshold (λ). This implies that the RSS variation of a link within the ellipse is inversely proportional to the link distance. This region reflects the area where objects can cause significant changes in the RSS due to scattering, diffraction, or absorption (Niroshan et al. 2018).

$$W_{l,i} = \begin{cases} d, & \text{if } d_{ij}^{(1)} + d_{ij}^{(2)} < d + \lambda \\ 0, & \text{otherwise} \end{cases} \tag{2.9}$$

- d : The distance between the two nodes,
- $d_{ij}^{(1)}$ and $d_{ij}^{(2)}$: The distances from the center of voxel j to the two node locations for link i,
- λ : The width of the ellipse. This is a tunable parameter.

Gaussian Model

The traditional ellipse model considers all voxels within a defined elliptical region equally. But the Gaussian model applies a Gaussian function to give higher weights to voxels that lie directly along the LOS between a transmitter and receiver. Voxels farther from this path are assigned progressively lower weights, based on their distance from the LOS. Figure 2.2c visualizes the Gaussian model and the corresponding equation is given as follows (Niroshan et al. 2018):

$$W_{l,i} = e^{-\frac{(d_{l,i}-d_l)^2}{2\sigma^2}} \tag{2.10}$$

- $d_{l,i}$: the sum of distances from the center of pixel i to the endpoints of the link.
- d_l: the length of the link l.

- σ: a pre-defined parameter.

Above models are based on several assumptions mentioned below,

- A person located on the link line causes attenuation
- The person affects the RSS measurements only when located near the link line.
- Environment is homogeneous.
- All the links experience the same propagation losses.

But in cluttered environments, the links experience different losses since they cover different spatial areas. A weight model considering the fade levels more accurately is proposed by Kaltiokallio, Bocca & Patwari (2014). However, these methods require prior knowledge of the monitored area.

A Fade Level-based Spatial Model

The fade level-based model is a method used to enhance the accuracy by accounting for variations in RSS due to environmental factors. It measures the difference between the observed mean RSS on a specific link and channel, and the expected RSS predicted by a radio propagation model (Eq. 2.11), such as the log-distance path loss model. This difference is called the fade level (Kaltiokallio, Bocca & Patwari 2014),

$$F_{c,l} = \bar{r}_{c,l} - P(d, c) \tag{2.11}$$

Where $P(d, c)$ is a model for the RSS as a function of distance and channel. In a wireless network, the RSS can be modeled, for example, using the log-distance path loss model:

$$P(d, c) = P_0(c) - 10\eta \log_{10} \left(\frac{d}{d_0} \right), \tag{2.12}$$

$P_0(c)$ is the transmit power-normalized reference loss on channel c, and η is the path loss exponent. This reflects how much a signal is attenuated or enhanced compared to what is theoretically expected.

Since λ is unique for each link and channel as explained above, the new weight model is expressed as:

$$w_{c,l,j}^{\delta} = \begin{cases} \frac{1}{n_j \cdot p^2}, & \text{if } d_{lj}^{\text{tx}} + d_{lj}^{\text{rx}} < d + \lambda_{c,l}^{\delta} \\ 0, & \text{otherwise} \end{cases} \tag{2.13}$$

Where $w_{c,l,j}^{\delta}$ is the weight of voxel j for link l on channel c for RSS sign δ. and n_j is the number of voxels within the ellipse of link l and p^2 is the area of a voxel.

Rather than the link distance and the fade level, another factor affecting the RSS value of a given distance is the position of the object compared to the links.

Gradual-Changing Weight Model

It has been observed that the impact of the object is higher when the distance between the person and either of the nodes is smaller (Fig 2.3a).

And according to the diffraction theory most EM energy affected by the object is spread in the first Fresnel zone. Therefore the influence of the target is very small when the target is outside the first Fresnel zone (Fig 2.3b).

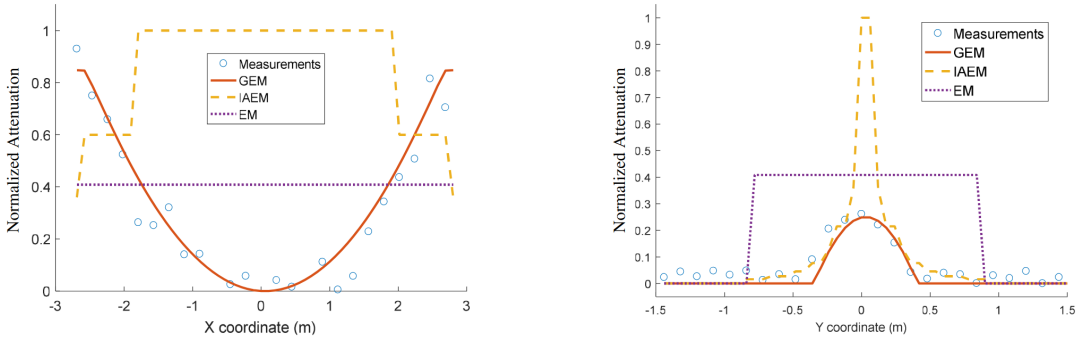

(a) (b)

Figure 2.3: (a) RSS variation along the free path (b) RSS variation across the free path (Adapted from Ke et al. (2019))

To accommodate them, the gradual-changing weight elliptical mode has been proposed as follows (Ke et al. 2019),

$$w_{ij} = \begin{cases} \frac{a_i - (d_{ij1} + d_{ij2})}{a_i - d_i} \times \frac{(d_{ij1} - d_{ij2})^2}{d_i^2} & \text{if } d_{ji1} + d_{ji2} < d_j + \rho_i^{\max} \\ 0 & \text{else} \end{cases} \tag{2.14}$$

where a_i is the length of the elliptical major axis on link i, and $\rho_i^{\max} = \sqrt{\lambda d_i/2}$ is the maximum first Fresnel radius. In this model, $\frac{(d_{ij1}-d_{ij2})^2}{d_i^2}$ represents the weight variation along the ith link direction, while $\frac{a_i-(d_{ij1}+d_{ij2})}{a_i-d_i}$ describes the weight variation along the vertical direction of link i.

Furthermore, Hamilton et al. (2014) proposed an inverse area elliptical model, in which the shadowing effect of a target on a wireless link is considered to be inversely proportional to the area of the smallest ellipse that encloses the target and has the transmitter and receiver as its foci.

In a different approach, Wang et al. (2016) introduced a Saddle Surface (SaS) model to characterize the relationship between link measurements and target location. This model also provides a probabilistic distribution indicating the likelihood of a target being present at any given point within the spatial impact region.

Additionally, Guo et al. (2013) proposed an exponential-Rayleigh model, which captures both large-scale attenuation through an exponential decay component and small-scale variations through Rayleigh fading, accounting for multi path effects.

A notable observation is that these weighting models primarily aim to improve the accuracy of RTI, while largely overlooking computational efficiency.

One major challenge in enabling real world device free localization deployments is managing the energy consumption and communication requirements of RF sensor networks. These networks typically involve deploying numerous sensors around the monitored area, which can be impractical or costly in certain applications. While much of the existing research has focused on improving localization accuracy, issues such as computational simplicity and overall system cost remain critical concerns. A promising direction to address some of these challenges is the utilization of unintentional EM radiation, which can potentially reduce both hardware requirements and energy consumption by leveraging ambient signals already present in the environment.

2.8 Electromagnetic Radiation

A typical home or office environments tend to be saturated with unintentional EM radiation as any electrical device emit an EM noise. These EM radiation are specific to device models as they are caused by an internal switching mechanism which is unique to the device (Mulder 2010). Individual device recognition is possible even for identical models with receiving antennas of high sensitivity. EM radiation vary depending on the state of the device whether it is in standby mode, turned off or moved (Zhao et al. 2015).

2.8.1 Generation of Electromagnetic Waves from Circuits

A changing electric current in a wire generates a varying magnetic field, which in turn induces an electric field. This continuous interaction between electric and magnetic fields propagates through space as an EM wave (Grdović et al. 2022).

This phenomenon is governed by the following fundamental laws of physics:

- Faraday's Law of Induction states that a changing magnetic field creates an electric field.
- Ampère's Law (with Maxwell's correction) states that a changing electric field creates a magnetic field

Complete set of equations describing EM waves are as follows when considered *E* as the electric field, *H* is the magnetic field, ρ_v is the volume charge density and *J* is the electric current density, ε and μ are permittivity and permeability constants in the air (Cui et al. 2020).

$$\nabla \cdot \mathbf{E} = \frac{\rho_v}{\varepsilon} \tag{2.15}$$

$$\nabla \cdot \mathbf{H} = 0 \tag{2.16}$$

$$\nabla \times \mathbf{E} = -\mu \frac{\partial \mathbf{H}}{\partial t} \tag{2.17}$$

$$\nabla \times \mathbf{H} = \mathbf{J} + \varepsilon \frac{\partial \mathbf{E}}{\partial t} \tag{2.18}$$

Digital circuits process data by rapidly switching currents on and off in clock circuits, data buses, and high-speed connections. These fluctuating currents generate equally fast-changing magnetic fields, which in turn induce electric fields. This continuous interplay between varying electric and magnetic fields within the circuit results in the emission of EM waves (Cui et al. 2020).

Circuits emit EM radiation starting at the fundamental clock frequency. The propagated EM wave consist of fundamental wave with clock frequency and its harmonics. Clock signals usually have a waveform with a duty ratio of around 50%. If the duty ratio is close to 50%, the signal comprises strong odd harmonics while the even harmonics tend to be weak (Ye et al. 2010).

The strength and amplitude of the generated EM waves depend on two key factors. The first is the rate of change of the magnetic field *H*, which is directly related to the rate of change of the current *i* (Cui et al. 2020). The second factor is the variation in current levels, which in turn depends on the CPU workload and the operation of the switch-mode power supply.

$$E_F \propto \frac{dH}{dt} \propto \frac{di}{dt}.$$

Literature records that characteristics of the EM radiation including shape of the signal, the rate at which EM signals are being emitted from the electronic device, a frequency or set of frequencies of the EM signal, and change in the frequency of the EM signal over a period of time can be detected from a distance (Beetner et al. 2008).

Computers may emit EM radiation of several ranges of the spectrum as visible light given off by the screen, infrared radiation given off by all parts of the computer due to their temperature, radio waves given off by the WiFi antenna and Bluetooth antenna, and EM radiation by electronic circuitry. Components emitting EM radiation are mainly power supply, Central Processing Unit (CPU), mainboard, hard disks, CD and DVD readers, WiFi and Bluetooth antenna (Sayakkara et al. 2020).

Above mentioned components and other peripheral devices connected to the computer usually operate in a fixed frequency or a frequency range defined by design. But power management techniques are employed in modern architectures to reduce

power consumption and amount of heat generated by the chip. Dynamic Voltage and Frequency Scaling (DVFS) is one such technique in which, the frequency of many system components including processor cores, memory system last level cache , and interconnect can be automatically adjusted based on the need (Nath & Tullsen 2017).

2.8.2 Propagation of Electromagnetic Radiation

The RSS of radio signals decreases as the distance between the transmitter and receiver increases. This phenomenon is known as path loss. The attenuation of radio signals due to path loss has been modeled by averaging the measured signal power over long time periods and across various locations at the same distance from the transmitter (Hekmat & Mieghem 2006).

The path loss model states that the received power P_a is a decreasing function of the distance d between the transmitter and the receiver, often represented by a power law:(Patwari & Agrawal 2008)

$$P_a(r) = c \cdot d^{-\eta} \tag{2.19}$$

where:

- c is a constant,
- η is the path loss exponent, which depends on the environment.

In urban areas, η can range from 2 to 6, depending on the density of buildings and obstacles (Hekmat & Mieghem 2006).

Shadowing is caused by obstacles between the transmitter and receiver that attenuate the signal power through absorption, reflection, scattering, and diffraction. Shadowing may partially or fully block a wireless signal, causing variations in RSS. It occurs over large distances compared to the signal wavelength and leads to slow changes in signal power. Shadowing is typically modeled using a log-normal distribution, meaning the signal attenuation varies randomly but follows a predictable pattern (Goldsmith 2005).

Fading refers to the rapid fluctuations in the RSS due to multi path propagation. It occurs when a transmitted signal takes multiple paths to reach the receiver due to reflection, diffraction, and scattering. These multiple signals can interfere constructively or destructively, causing the received signal to vary over small distances and short time periods.

Unlike fading, which results from multi path interference and changes rapidly, shadowing is caused by large-scale environmental obstructions and varies more gradually.

There are three main models recorded in literature to model propagation of EM radiation considering path loss, fading and shadowing (Patwari & Agrawal 2008).

- Circular coverage model
- i.i.d. link fading model
- i.i.d. log-normal shadowing model

Circular Coverage Model assumes that each transmitter has a fixed circular range where the signal can be received. It does not account for obstacles or variations in the environment.

In i.i.d. Link Fading Model each link experiences independent random fading due to reflections, refractions, and diffraction. This model represent multi path effects, where signals take multiple paths to reach the receiver.

i.i.d. Log-Normal Shadowing Model assumes that shadowing (blocking effects) follows a log-normal distribution. This models the random attenuation of the signal due to large obstacles by taking to account environmental variations in signal propagation.

2.8.3 Literature related to Electromagnetic Radiation

Records of prior research exist related to near-field EM radiation detection, profiling electronic devices and EM tomography with a source and limited area that answer some questions that are considered limitations of this research.

A system for identifying devices using EM emissions from electronic devices is proposed by Beetner et al. (2008). They have utilized a classification based method

to identify unique characteristics of the unintentional EM signal emitted from selected electronic devices including computers, cell phones, two way radios and toy trucks, etc.

The possibility of detecting activity performed by a user was explored in Sayakkara et al. (2020). Authors have presented a methodology to identify the frequency channels from a high dimensional EM data set that leak software behavior related information and using random forest Machine Learning (ML) method classification of software activities was achieved.

Another interesting work records 3D EM tomography imaging with single layer sensor array. The sensor array includes a different number of coils,—8, 12 and 16, to conduct simulations. The conjugate gradient iterative method has been used in image reconstruction (Yue et al. 2021).

2.8.4 IQ Data

IQ data is a more accurate representation of a signal considering the signal as a combination of cosine functions. Rather than recording a signal as a series of momentary amplitudes, IQ data indicated the signal's position in a wave form at a given point in time (Q Kuisma 2023).

- I - In-Phase signal component
- Q - Quadrature signal component

Several characteristics of the data can be derived from a IQ data series using following equations (Q Kuisma 2023).

$$A(Amplitude) = \sqrt{I^2 + Q^2} \tag{2.20}$$

$$\phi(Phase) = \arctan\left(\frac{Q}{I}\right) \tag{2.21}$$

$$\text{RF power} = P(\text{dBm}) = 10 \times \log_{10}\left(10 \times (I^2 + Q^2)\right) \tag{2.22}$$

I indicates the specific height of the signal at a given point in time. Q is the also the value of waves' height when shifted by 90 degrees behind I. A single IQ sample is

taken at one point of time and contains both I and Q values. Each sample is reading the electrical energy coming off the antenna at that exact instant.

2.8.5 Signal Processing Methods

Signal we come across in this research are of two types (POLIKAR & Lu 1996).

- Stationary : Signals whose frequency content do not change in time (the signal either has a single frequency or all frequency components exist at all times)
- Non - stationary : frequency content change over time

Fast Fourier Transformation (FFT) is signal processing technique that suit best for stationary signals or if the time dimensional details of the signal is not required. Short Time Fourier Transformation (STFT) and Wavelet transformations can be applied to obtain the time dimensional details from non stationary details.

Summary of the transformations addressed are as follows (POLIKAR & Lu 1996, Lichtman 2024),

Transformation	**Function**	**Drawback**
FFT	Gives frequency content of the signal	No information about where in time those frequencies appear
STFT	Provides time-frequency representation with fixed resolution; shows which frequencies are present in each time window	Gives a fixed resolution at all times
Wavelet	Gives a variable resolution; shows what frequencies are most prominent around a time	Does not provide a uniform resolution across all frequencies (resolution varies with frequency)

Table 2.3: Characteristics of Signal Transformations

Fast Fourier Transformation

FFT converts a time-domain signal into its frequency components, allowing us to analyze the signal's frequency content. However, FFT does not indicate where in time a frequency

component appears (Lichtman 2024).

Consider a signal represented as a series of complex IQ samples, $x(t)$.

Procedure of FFT algorithm,

1. Select a frequency f to analyze: Define a complex sinusoidal signal at the chosen frequency f:

$$e^{j2\pi ft} = \cos(2\pi ft) + j\sin(2\pi ft)$$

where j is the imaginary unit.

2. Multiply the original signal with the complex expression of f: Given the complex IQ samples of the original signal, $x(t)$, we can multiply $x(t)$ by the complex sinusoid at frequency f:

$$x(t) \cdot (\cos(2\pi ft) + j\sin(2\pi ft))$$

This multiplication isolates the component of the signal that resonates at frequency f. If the frequency component f is present in $x(t)$, this product will yield a non-zero value; otherwise, it will yield zero.

3. Integrate the product over time: To determine the dominance of the selected frequency f in the signal, integrate this product over time:

$$\int x(t) \cdot (\cos(2\pi ft) + j\sin(2\pi ft))\ dt$$

The result of this integral is proportional to the dominance of the selected frequency f within the complex signal $x(t)$.

Short Time Fourier Transformation

This algorithm apply FFT to a non stationary signal by assuming that parts of the signal are stationary.

STFT divides the signal into short time frames, each of which is analyzed separately. But cutting the signal into segments without smoothing the edges can introduce errors, such as spectral leakage, due to the sudden changes at the segment boundaries. A

window function helps to reduce these by gradually fades the segment's edges to make the transition smooth (POLIKAR & Lu 1996).

There are several window functions in use :

- Rectangular Window: Simple "on/off" window without tapering, but can cause significant spectral leakage.
- Hann (Hanning) Window: Tapers to zero at both ends, reducing spectral leakage.
- Hamming Window: Similar to the Hann window but tapers slightly differently. useful for reducing side lobes in the frequency domain.
- Gaussian Window: Provides a smooth, bell-shaped curve; good for time-frequency localization.
- Blackman Window: Provides more tapering than the Hann and Hamming windows, further reducing spectral leakage.

Procedure of STFT algorithm,

1. Define the window size and function: Choose a window function $w(t)$ with a specified size τ, which determines the portion of the signal analyzed at each time step.

2. Set initial time $t = 0$: For each time point t, multiply the signal $x(t)$ within the window size τ by the window function $w(t)$:

$$x(t) \cdot w(t - \tau)$$

3. Apply the Fourier Transform to the windowed segment:

$$X(t, f) = \int_{-\infty}^{\infty} x(\tau)\, w(\tau - t)\, e^{-j2\pi f \tau}\, d\tau$$

4. Integrate over time: By repeating this process across the time axis, we obtain a time-frequency representation:

$$\text{STFT}(t, f) = \int x(t) \cdot w(t - \tau)\, e^{-j2\pi f t}\, dt$$

This results in a time-frequency representation that shows how the frequency content of the signal varies over time.

Problem with STFT is the resolution, caused by the Heisenberg Uncertainty Principle (POLIKAR & Lu 1996).

Heisenberg Uncertainty Principle

States that the momentum and the position of a moving particle cannot be known simultaneously.

In signal processing it applies as follows, We cannot know what frequency exists at any given time instant. The best we can do is to estimate what frequency bandwidth exists at any given interval of time. This is a problem of resolution.

Wavelet Transformation

The continuous Wavelet Transformation (WT) was developed as an alternative approach to the STFT to overcome the resolution problem.

The algorithm passes the given time domain signal from various high pass and low pass filters, which filters out either high frequency or low frequency portions of the signal. This outputs frequencies that resonates with the filter in time domain.

Fundamental idea in WT is that high frequency components can be located better in time but has low frequency resolution as they change quickly and low frequencies has better frequency resolution and poor time resolution as they are slow to change (POLIKAR & Lu 1996).

Differences between the STFT and the WT (POLIKAR & Lu 1996):

- The Fourier transforms of the windowed signals are not taken, and therefore a single peak will be seen corresponding to a sinusoid.
- The width of the window is changed as the transform is computed for every single spectral component,

Explanation of some terminologies,

1. Wavelet: A wavelet is a short ”wave” with a start and end. Unlike a sine wave that goes on forever, a wavelet has a limited length.

2. Mother Wavelet: The mother wavelet is the main wavelet shape or pattern that used to create other wavelets. By stretching or compressing by changing the scale, different ”child” wavelets are made to analyze the signal.

3. Scale : A parameter similar to zoom level. Large scale stretches the wavelet and reduces the frequency. This reveals low-frequencies and broad features in the signal. With contrast to that small scale compresses the signal revealing high-frequencies and detailed features in the signal.

4. Translation (Shifting the Wavelet): Translation means moving the wavelet to different positions along the signal, like sliding a window across a signal.

Procedure of WT algorithm

1. Choose a wavelet function $\psi(t)$ and parameters for scale a and translation b.

2. For each value of b, the wavelet $\psi(t-b)$ is centered at b, allowing it to capture local features of the signal around that point.

- In Continuous Wavelet Transform (CWT), b varies continuously over the time domain of the signal. - In Discrete Wavelet Transform (DWT), b varies in discrete steps, determined by the decomposition level.

3. Adjust the wavelet's frequency response by scaling:

$$\psi_{a,b}(t) = \frac{1}{\sqrt{a}}\psi\left(\frac{t-b}{a}\right)$$

4. Calculate the Continuous Wavelet Transform (CWT)**: The CWT of a signal $y(t)$ is calculated by measuring the similarity between $y(t)$ and the shifted, scaled wavelet $\psi_{a,b}$. This is given by:

$$C(a,b) = \int_{-\infty}^{\infty} y(t)\,\psi^*_{a,b}(t)\,dt$$

where $\psi^*_{a,b}(t)$ is the complex conjugate of $\psi_{a,b}(t)$. Large values of $C(a,b)$ indicate a strong match, showing that the wavelet captures significant features of the signal at the specific time b and scale a.

5. Calculate the Wavelet Coefficient: The area under the curve (the sum of positive and negative contributions) gives the wavelet coefficient for a specific scale a and

translation b. This coefficient measures the degree to which the wavelet represents the signal at that time and scale.

6. Repeat for Different Translations, b: Move the wavelet along the time axis, b, and calculate the corresponding coefficients. This provides a set of coefficients that represent how the signal varies with time at the given scale a.

7. Repeat for Different Scales, a: Change the scale a to capture different frequency components of the signal, repeating the analysis for each scale.

8. Construct a Time-Scale Map: A time-scale map visualizes the wavelet coefficients $C(a, b)$ as a function of both time b and scale a. This map provides insight into how the signal's frequency content changes over time.

2.8.6 Representations of the signal

There are multiple statistical representation for a given set of signal data including mean, median and mode.

Representation	**Pros**	**Cons**
Mean	Provides a better representation for continuous data, such as IQ values. Commonly used for normally distributed data.	Sensitive to outliers, which can distort the representation. Not ideal if the data distribution is skewed.
Median	Less affected by outliers compared to the mean. A better measure of central tendency when the distribution is skewed.	Still somewhat influenced by outliers, though to a lesser extent than the mean.
Mode	Represents the most frequent value, useful in identifying dominant signal strength in noisy environments. Best suited for categorical or discrete data.	Less effective for continuous data like IQ scores.

Table 2.4: Comparison of Mean, Median, and Mode for Data Representation

Signal to Noise Ratio

The Sound to Noise Ratio (SNR) is a method used to quantify how much the useful signal stands out compared to background noise. There are different methods of calculating SNR tailored to specific applications and available data (Lyons 2011, *Signal-to-noise ratio* 2024).

Power Ratio Method

The classic definition mostly used in electrical engineering and telecommunications.

$$SNR = 10 \cdot \log_{10} \left(\frac{P_{\text{signal}}}{P_{\text{noise}}} \right)$$

Amplitude Ratio Method

This method is used when signal and noise are measured as amplitudes such as in voltages or currents.

$$SNR = 20 \cdot \log_{10} \left(\frac{A_{\text{signal}}}{A_{\text{noise}}} \right)$$

Mean to Standard Deviation Ratio

This method is used in scenarios when the noise is variable due to randomness and unpredictability.

$$SNR = \frac{\mu}{\sigma}$$

The standard deviation (σ) is a measure of how much the noise deviates from its mean value. Higher variance indicates more fluctuations, leading to a noisier signal and lower SNR. In contrast lower variance gives higher SNR and a more stable signal. The noise can be due to thermal effects, electronic components, environmental factors, or interference. To apply this method, noise is assumed to be gaussian and that the mean of the signal is mainly influenced by the desired signal rather than the noise.

Two separate signals are required in power ratio method and amplitude ratio method to be able to clearly separate the noise or filtering is required if noise is embedded in the signal to separate noise.

When the pure signal and the noise can not be separately known and only the measured signal is available, Mean to standard deviation ratio can be applied.

Chapter 3

Design and Methodology

3.1 Research Approach

This is an experimental research adapting a quantitative approach. Data is collected by capturing EM radiations, which reveal interferences caused by static objects. These signals are then analyzed to determine how the objects alter the field. This approach follows an inductive research strategy, deriving insights from collected data.

3.2 Setup

The initial step prepares the experimental setup. Required components and software to build the setup are as follows,

1. HackRF
2. Directional Antenna
3. GNU Radio Companion

Captured EM waves will be processed by GNU Radio Companion and stored as an In-phase and Quadrature (IQ) dataset. Required datasets will be collected in several instances considering the location of the object, signal receiver and the CPU workload.

This research focuses on EM radiation, which is inherently invisible and intangible. A key challenge in detecting EM radiation emitted by a device is identifying unique

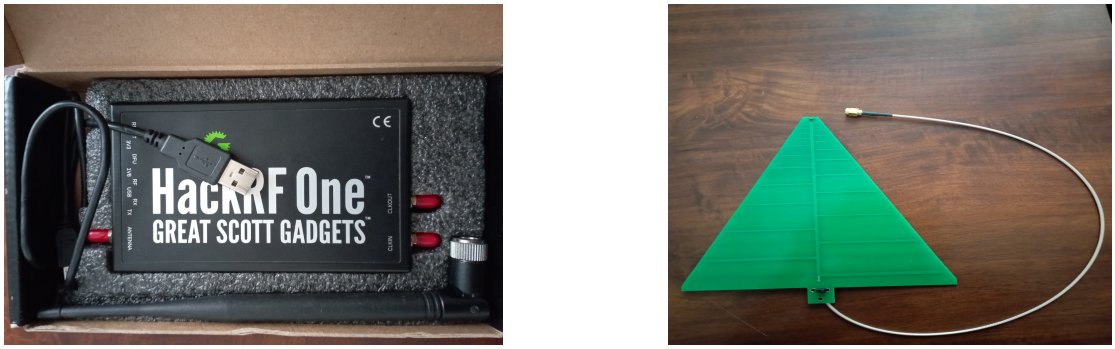

(a) (b)

Figure 3.1: Components of the setup (a) HackRF (b) Directional antenna

patterns of radiation corresponding to specific incidents, such as fluctuations in CPU workload or the device's power state (e.g., turning the device on or off). To address this, the experimental setup outlined in Figure 3.2 was designed to monitor these variations effectively. The antenna, signal source and signal receiver are positioned horizontally at a height of 0.75 m.

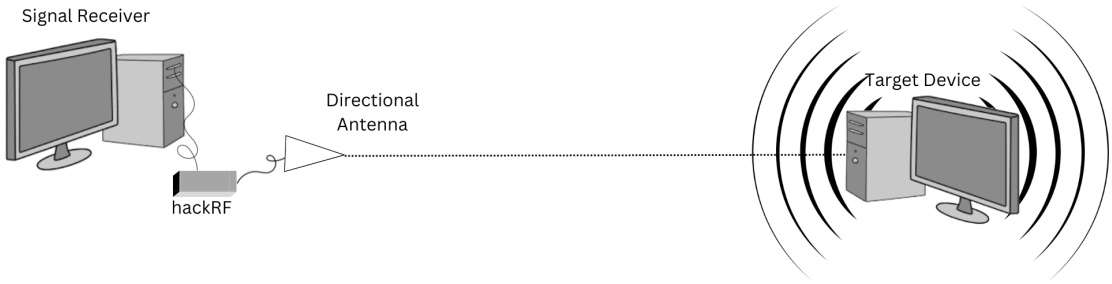

Figure 3.2: Simple setup to obtain IQ data

The signal source is a desktop computer with Intel(R) Core(TM) i5-7400 CPU and a Corsair CX450M switch-mode power supply unit.

To study these EM emissions systematically, a controlled signal generation procedure is required. The CPU workload is manipulated using the `stress-ng` tool in a Linux environment, which allows precise control over the processing load and corresponding

EM emission. The CPU clock frequency is monitored when required using the `htop` command.

Signals are captured by a laptop running GNU Radio software, connected to a HackRF One device for signal sampling. Mainly two GNU flow graphs were used to store (Figure 3.4a) and playback (Figure 3.4b) data. A far-field antenna is employed to collect the emitted radiation. The RSS is visualized through the `fosphor sink` block in GNU Radio, and the data is stored in `float32` format for further analysis.

An example of the experimental setup in a controlled lab environment is shown in Figure 3.3.

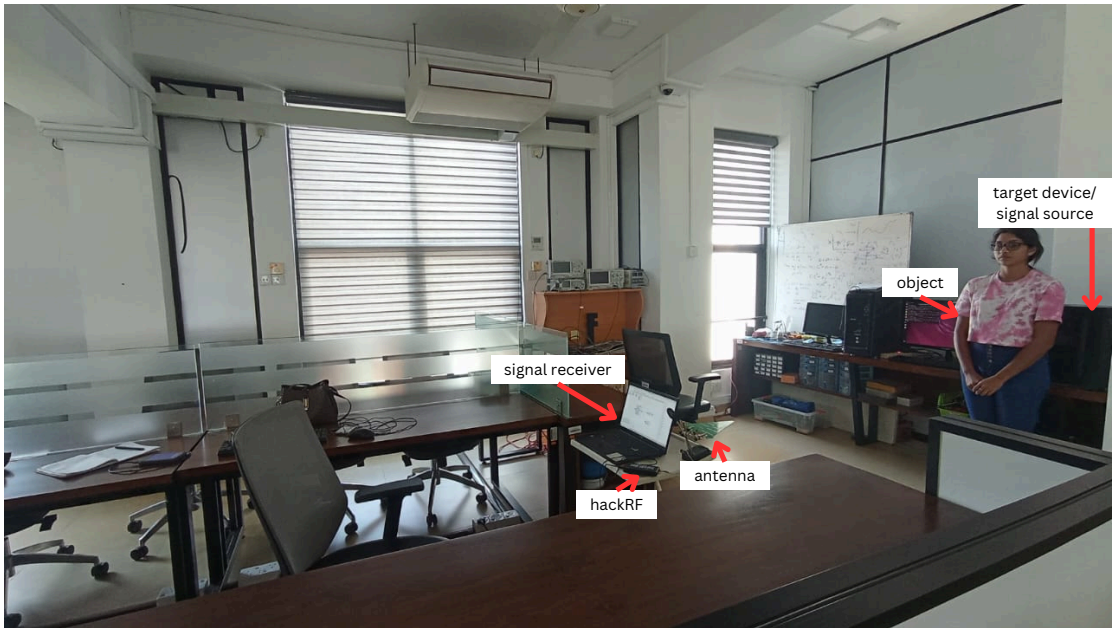

Figure 3.3: Position of components for experiment setup

Stress Tool

The `stress-ng` is a benchmarking and stress-testing utility designed to apply controlled load to various system resources, including the CPU, memory, and I/O subsystems. It achieves this by executing specific "stressors" that simulate high-load scenarios, allowing for thorough performance evaluation under stress conditions.

The following command was used in the experiments to create different levels of load on the system:

```
stress-ng --cpu 4 --cpu-workload 100 --io 2 --vm 1
--vm-bytes 1G --timeout 10s
```

This command initiate specific stressors to load the CPU, memory, and I/O systems, with the `--cpu` flag specifying the number of CPU cores to be stressed, `--cpu-workload` defining the level of CPU workload, and `--vm` and `--vm-bytes` setting the virtual memory allocation. The `--timeout` option ensures the stress test runs for a specified duration.

The CPU workload is monitored using the `htop` command, which provides real-time resource usage statistics. Additionally, the system's CPU frequency is tracked using the command `watch -n1 "grep Hz /proc/cpuinfo"` to observe any variations in clock speed during the stress tests.

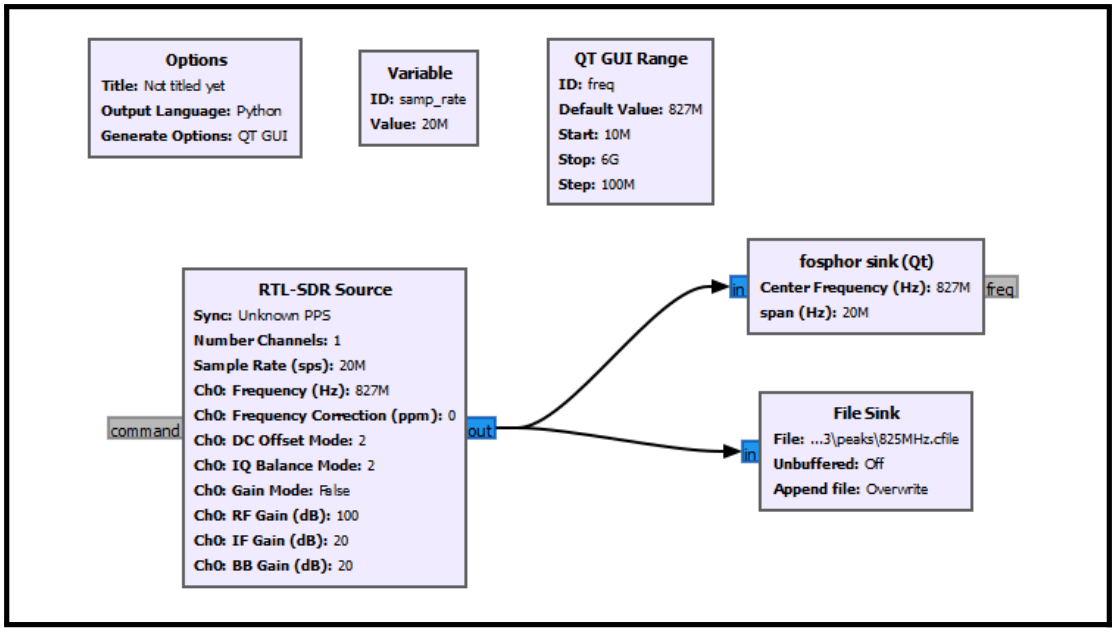

(a)

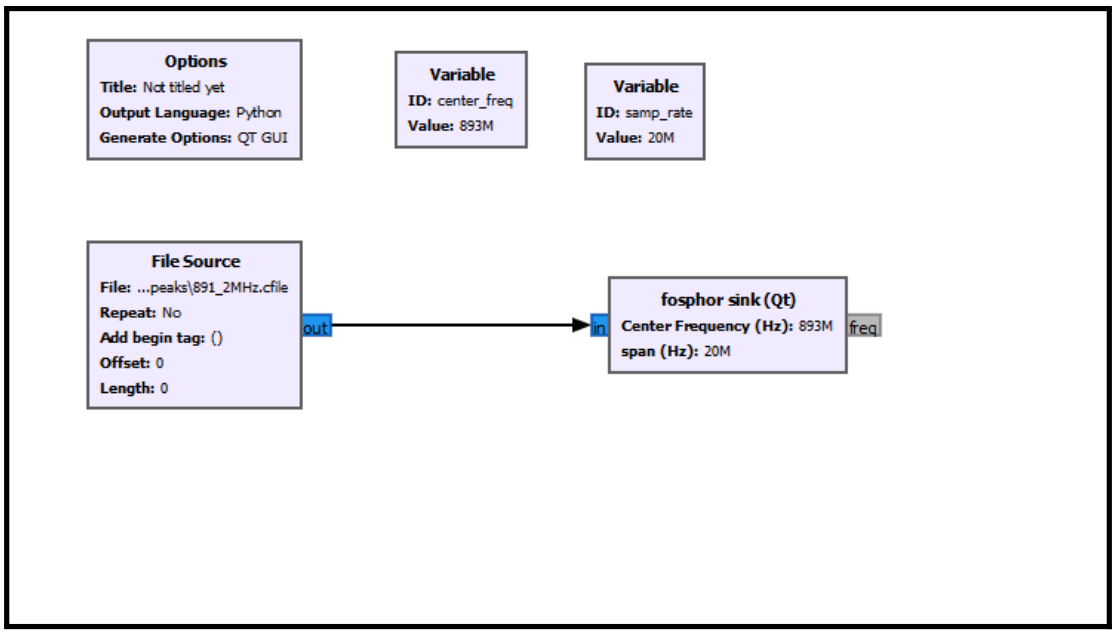

(b)

Figure 3.4: GNU flow graphs (a) To record IQ data (b) To playback IQ data

3.3 Data Collection and Preprocessing

Data was collected over a 30 second period at each step with a sampling rate of 20 MHz and stored in a `.cfile` format with `float32` precision.

The raw data was initially converted into IQ format and then processed using STFT, implemented through Python's spectrogram function. The STFT was chosen among other signal transformation techniques due to its ability to capture time-varying changes in signal strength at a selected frequency. The median value of signal strength within the relevant frequency bin was computed to represent the signal at each time instance.

Collected data contained outliers due to ambient noise in the surrounding environment. Additionally, it was noted that the histograms of each instance were not perfectly symmetric, indicating potential skewness in the distribution. As a result, the median was selected as the central measure of tendency, in preference to the mean or mode, to eliminate the influence of outliers and asymmetry. To further analyze the data, several visualization techniques were employed, including Power Spectral Density (PSD) plots, FFT plots, spectrograms, and histograms.

Chapter 4

Experiments and Results

4.1 Preliminary Signal Analysis

4.1.1 Experiment: Identification of Harmonics of 33 MHz to Use as the Target Frequency

The `lshw` command in Linux provides detailed information about the hardware configuration of a computer, including the clock frequencies of its components. The results of running this command on the signal source are summarized in Table 4.1.

Steps :

1. Use the `lshw` command to identify the operating frequencies of the hardware components connected to the signal source.

2. Program the harmonics of the selected operating frequency, close to the center frequency of the flow graph shown in Figure 3.4a. This is because of the unavoidable circuit noise recorded at the center frequency.

3. Observe the signal strength when the signal source is off, idle, and under maximum CPU workload.

Observations :

The clock frequencies of the hardware components were observed to be 3 GHz, 33 MHz, and 66 MHz. Among these, 3 GHz represents the maximum operating frequency of the CPU, which fluctuates frequently due to DVFS in order to conserve

Component	Description	Clock Speed
CPU	Intel(R) Core(TM) i5-7400 CPU	3.00GHz
Host bridge	Xeon E3-1200 v6/7th Gen Core Processor Host Bridge/DRAM Registers	33MHz
VGA controller	HD Graphics 630	33MHz
System peripheral	Xeon E3-1200 v5/v6 / E3-1500 v5 / 6th/7th/8th Gen Core Processor Gaussian Mixture Model	33MHz
USB controller	200 Series/Z370 Chipset Family USB 3.0 xHCI Controller	33MHz
Signal processing	200 Series PCH Thermal Subsystem	33MHz
Communication controller	200 Series PCH CSME HECI #1	33MHz
SATA controller	200 Series PCH SATA controller [AHCI mode]	66MHz
PCI bridge	200 Series PCH PCI Express Root Port #5	33MHz
USB controller	ASM2142 USB 3.1 Host Controller	33MHz
NVMe device	Samsung SSD 960 EVO 250GB	33MHz
ISA bridge	200 Series PCH LPC Controller (B250)	33MHz
Memory controller	200 Series/Z370 Chipset Family Power Management Controller	33MHz
Audio device	200 Series PCH HD Audio	33MHz
SMBus	200 Series/Z370 Chipset Family SMBus Controller	33MHz
Ethernet	Ethernet Connection (2) I219-V	33MHz

Table 4.1: Hardware Specifications Table

power. Based on this, 33 MHz was identified as the dominant frequency at which key components of the signal source operate. The harmonics of this frequency were examined to determine a suitable target frequency from the previously observed frequency ranges.

Each harmonic of 33 MHz within the signal range of HackRF was monitored to detect changes in signal strength when the desktop was off, idle, and under 100% CPU workload. This analysis led to the identification of the 24th harmonic (792 MHz) and the 25th harmonic (825 MHz) as the most reliable indicators of EM radiation from the device.

Further investigation revealed that the 20 MHz frequency bandwidth centered around the target frequencies is sensitive to changes in the signal source. Among these, the 792 MHz frequency band was found to be more sensitive than the 825 MHz frequency band, making it a better candidate for tracking EM radiation.

When using GNU Radio flow graphs, it is important to set the target frequency close to, but not exactly at the center frequency, to minimize issues like DC offset and leakage from the local oscillator.

4.2 Distance and Environmental Factors

4.2.1 Experiment:Determining the Maximum Distance to Detect EM radiation from the Signal Source

This experiment was conducted in various environments to determine the maximum distance at which EM radiation emitted from the signal source can be captured, allowing to detect the presence of an object.

Steps :

1. Position the signal source stationary and set to operate at the maximum workload.

2. Execute the flow graph (Figure3.4a) in GNU Radio Companion on the signal-receiving laptop and collect data for 30 seconds.

3. Repeat step 2 with and without the object placed between the signal source and the receiver.

4. Increase the distance between the signal source and the receiver and repeat step 3 at each new distance.

5. Preprocess the collected data and plot the results.

Observation : The experiment was conducted in three different environments: an outdoor open ground, an indoor empty room, and an indoor working environment. It was observed that the RSS decreased with distance, but only up to a certain point. Beyond this distance, the effects of multi path interference became apparent, and the influence of nearby objects on the received signal became increasingly unpredictable.

(a)

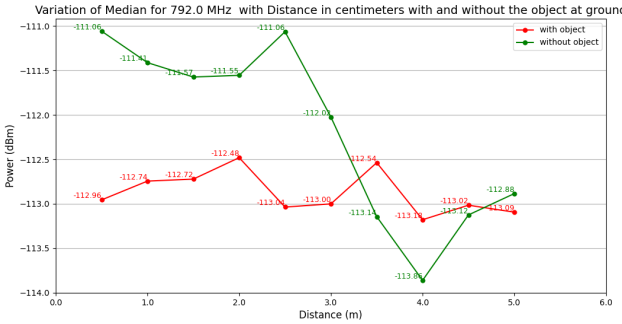

(b)

Figure 4.1: Outdoor open ground environment (a) Experiment setup (b) Variation of median over distance with and without object on the signal link

(a)

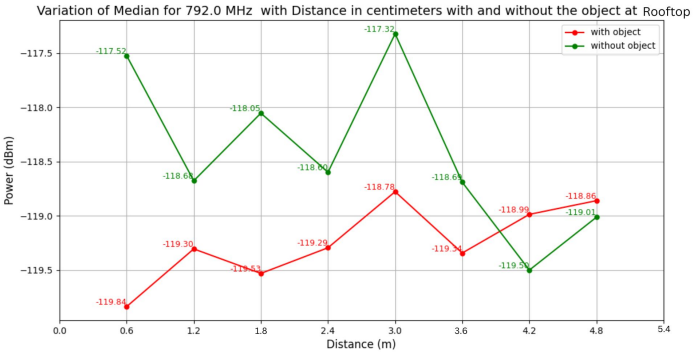

(b)

Figure 4.2: Indoor empty environment (a) Experiment setup (b) Variation of median over distance with and without object on the signal link

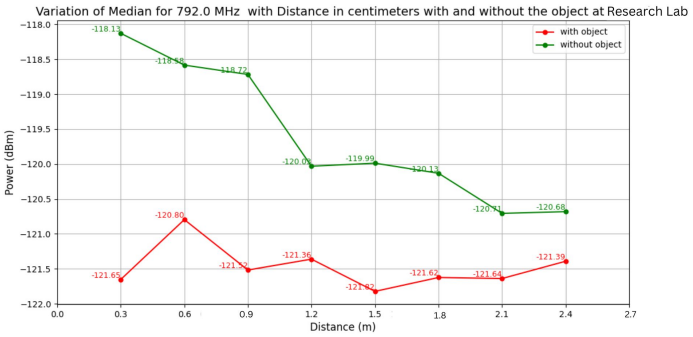

(a) (b)

Figure 4.3: Indoor working environment (a) Experiment setup (b) Variation of median over distance with and without object on the signal link

4.3 Effect of CPU Workload

4.3.1 Experiment: Study the Effect on Transmitted Signal Power by an Object Placed Between the Signal Source and the Signal Receiver with Different CPU Workloads

The signal source in this experiment uses an Intel® Core i3-3GHz microprocessor with DVFS technology. As a result, the CPU frequency dynamically adjusts with the workload to optimize power efficiency. The EM radiation from the signal source is primarily influenced by the power supply and bus communication, both of which depend on the CPU frequency. Therefore, the EM radiation emitted by the device was observed by positioning the signal receiver stationary at a distance of 2.1 m from the signal source while using the `stress-ng` tool to control the CPU workload.

Steps :

1. Position the signal source and signal receiver stationary at a constant distance (2.1 m).

2. Adjust the CPU workload of the signal source by using the following `stress-ng` command: `stress-ng--cpu 4 --cpu-workload x --io 2 --vm 1 --vm-bytes 1G --timeout 30s`

Here, the value of x represents the CPU workload percentage, which is varied

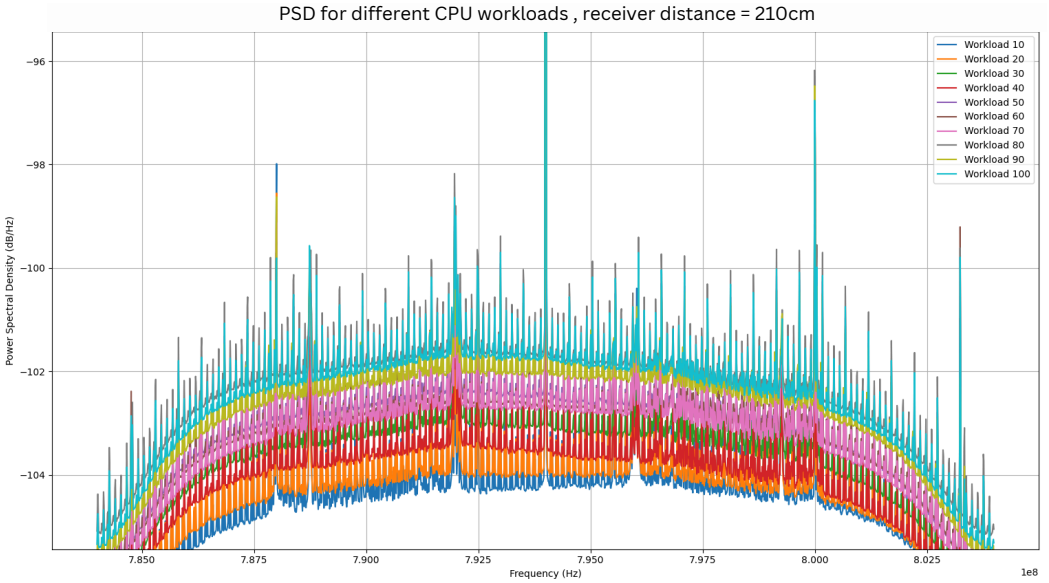

Figure 4.4: Variation of Power Spectral Density for Different CPU Workloads captured at 2.1 m from signal source and target signal 792 MHz

throughout the experiment.

3. Place an object between the signal source and the signal receiver, approximately 0.3 m from the receiver, and repeat step 2 for each specified CPU workload.

4. Collect data for 30 seconds with and without the object and plot the PSD to compare the effects.

Observations : The CPU workload was increased incrementally by 10% at each step. PSD plots were generated using the `psd` function from Python's Matplotlib library to visualize the signal strength across different frequency components. The results, as shown in Figure 4.4, indicate that the strength of the received signal spectrum varies significantly with changes in CPU workload.

Furthermore, the presence of the object between the signal source and receiver caused a considerable reduction in the observed signal strength at all CPU workload levels. This drop in signal strength is indicative of the object's interference, which attenuates the transmitted signal as the CPU workload increases.

4.4 Effect of an object on Electromagnetic Radiation

From above experiments, three primary factors were identified as significantly influencing the RSS:

- Transmitted signal strength (This depends on CPU workload)
- The location of the object relative to the signal path
- The distance between the signal receiver and the signal source.

In the following experiments CPU workload was maintained 100% at all times as it was observed that high CPU workloads emit stronger radiations (Figure 4.4). To isolate the effect of each factor on RSS, one variable was adjusted while the others remained constant.

4.4.1 Experiment: Study the Effect on Received Signal Strength by a Stationary Object Placed Between the Signal Source and the Signal Receiver

The objective of this experiment was to investigate whether the RSS changes when a stationary object is placed between the EM radiation source and the signal receiver.

Steps :

1. Position the object 0.3 m away from the signal source (Figure 4.5a).

2. Collect data for 30 seconds at each distance for the following scenarios:

Scenario 1: The desktop is turned off to establish a baseline signal strength (no active source).

Scenario 2: The desktop is on, and the object is not placed between the source and receiver.

Scenario 3: The object is placed between the source and receiver.

3. Repeat steps 1 and 2 for distances ranging from 0.6 m to 2.7 m, increasing the distance by 0.3 m at each step.

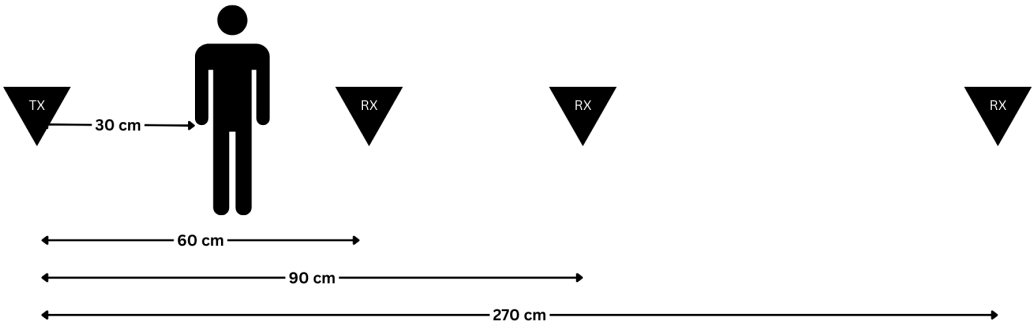

(a)

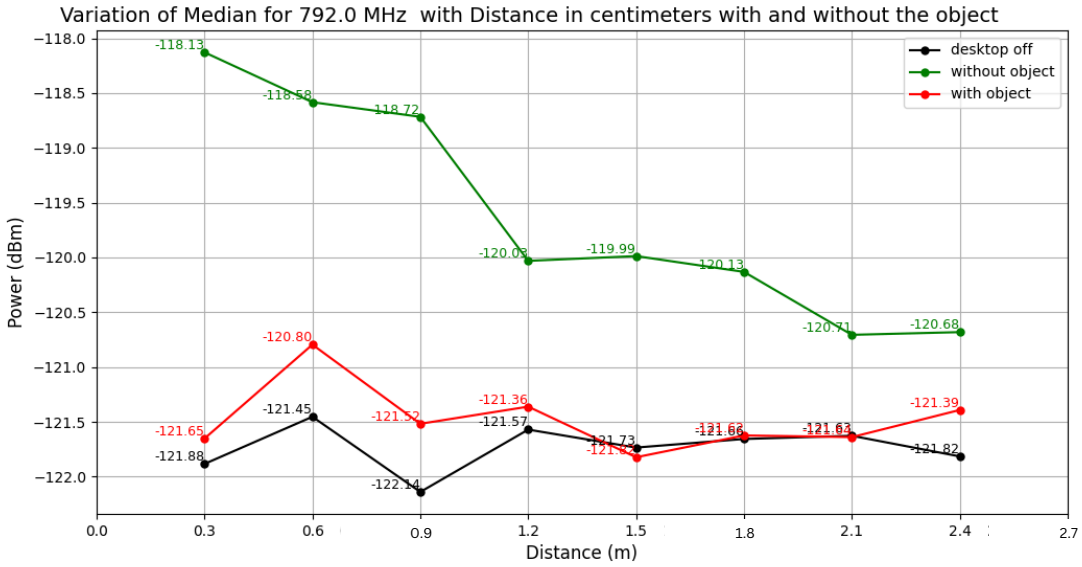

(b)

Figure 4.5: Experiment 4 (a) Setup (b) Variation of median RSS (792 MHz) with distance, with the object stationary at 0.3 m from the receiver and target signal 792 MHz.

Observations :

Theocratically RSS decreases with distance by $1/d^2$. The graph without the object in Figure 4.5b indicates that in free space propagation, radiation emitted from the signal source agrees with the theory. The graph when the desktop is off in Figure 4.5b indicates the noise level when the signal source is turned off. The RSS decreases When the object

is placed in between the signal source and the signal receiver and it is blocking almost all the radiation when the object placed closed to the signal source and the change in signal can be detected as far as from 2.7 m. But as the distance increases, the impact of the object on signal attenuation decreases.

4.4.2 Experiment: Study the Effect on Received Signal Strength as an Object Moves Toward a Stationary Signal Receiver

This experiment was conducted to examine how the movement of an object toward a stationary signal receiver affects the RSS.

Steps:

1. Position the signal source and receiver stationary 2.1 m apart, with the object initially placed 0.3 m away from the signal source (4.6a).

2. Collect data for 30 seconds at each distance for the following scenarios:

Scenario 1: The desktop is turned off to establish a baseline signal strength (no active radiation source).

Scenario 2: The desktop is on, and the object is not placed between the source and receiver.

Scenario 3: The object is placed between the source and receiver.

3. Repeat steps 1 and 2, increasing the distance between the signal source and the object by 0.3 m at each step.

The collected data was plotted against distance, with the median value used to represent the data. The results obtained are shown in Figure 4.6b.

Observations:

The data confirms that the object's influence on the received signal is high when it is closer to the receiver or the source and less when the object is at the center.

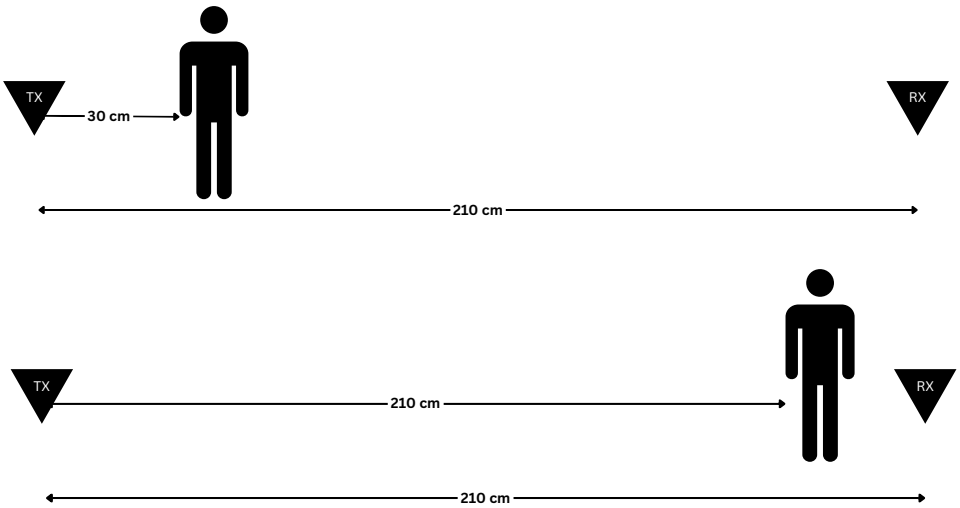

(a)

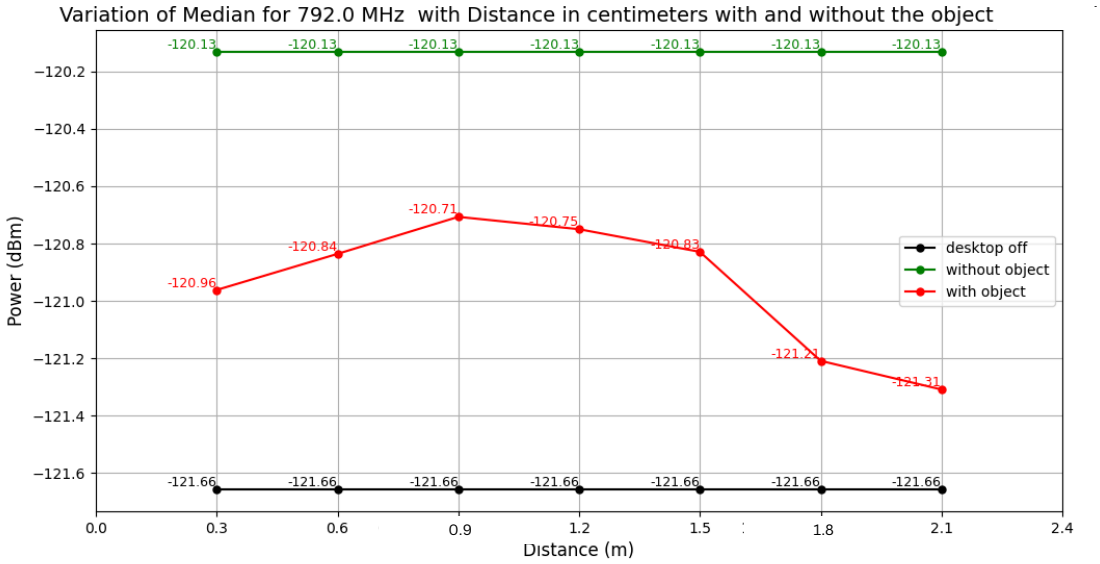

(b)

Figure 4.6: Experiment 5 (a) Setup (b) Variation of median RSS (792 MHz) with distance as the object moves toward the receiver and target signal 792 MHz.

Chapter 5

Analysis and Discussion

A key distinction between this research and other similar studies is that the target signal in this work is an unintentional EM side channel radiation, rather than a deliberately emitted signal from a purpose-built transmitter. As such, there are several important considerations when utilizing the unintentional EM radiation emitted by electronic devices for applications such as tomography.

The critical factors to be understood before leveraging these unintentional EM emissions are:

- The frequency range of EM radiation emitted by the device
- The maximum distance to detect EM radiation emitted by the device
- The effect of an object on the EM radiation emitted by the device

The experiments in this research specifically address these key requirements. The preliminary experiments focused on identifying the signal range for analysis, while subsequent experiments studied the influence of distance and environmental factors on the detection of these signals. After gaining an understanding of the characteristics and behavior of EM radiation, further experiments were conducted to study the effect of objects on the emitted EM radiaiton.

EM radiation represent a form of energy that is invisible and intangible. As such, the presence of these radiation can only be detected when they are active or when their

energy is transferred into a detectable form. In this research, we utilize a far-field antenna and a Software Defined Radio (SDR) half-duplex transceiver to convert the EM radiation into an electrical current for further analysis.

The CPU controls current flow within its own internal circuits, and also directs the flow of data and instructions. This process affects the flow of current to other components in the computer system and power input through the Power Supply Unit (PSU) (Gough et al. 2015). The current flow in these components corresponds to this operating frequency and which in turn generates a changing magnetic field inducing and electromotive force (Cui et al. 2020). Therefore the EM radiation emitted from a computing device may have a wide range of frequencies.

However, since the signal source's CPU employs DVFS technology, the CPU frequency changes with the workload. Therefore, the observed signal ranges do not solely correlate with EM radiation emitted by the CPU. Instead, the ranges display variations associated with any CPU workload, indicating that the emitted EM radiation is influenced by factors beyond the CPU. To further investigate this, Experiment 4.1.1 was conducted to identify the operating frequencies of the various components within the signal source.

An analysis of the hardware characteristics of the components connected to the signal source revealed that aside from the CPU, most components operate at a frequency of 33 MHz. Given that signals emitted from the source can contain higher-order harmonics, Experiment 4.1.1 focused on examining the 33 MHz fundamental frequency and its harmonics. Changes in signal strength were observed for different CPU workloads and the on/off status of the device. It was found that the 24th harmonic (792 MHz) demonstrated the highest sensitivity to changes in the CPU workload, making it the most suitable target frequency. However, it is important to note that EM radiation from the device is not limited to a single frequency; rather, it spans an observable 20 MHz bandwidth, with the narrow band centered around 792 MHz exhibiting the highest sensitivity.

A key factor in using EM radiation for tomography is determining the maximum

distance at which these radiation can be detected. Experiment 4.2.1 was designed to address this by testing detection capabilities in different environments: an outdoor ground, an indoor empty environment, and an indoor working environment. These environments were chosen to evaluate the maximum distance between the signal source and the receiver, as well as to assess the impact of external noise sources such as other electronic devices, moving objects, and static obstacles. In the outdoor and indoor empty environments, external noise sources and static obstacles were minimized, whereas the indoor working environment included static objects to study the effects of multi path propagation in a more realistic, cluttered setting.

The distance between the signal source and the signal receiver was gradually increased while keeping the signal source stationary. As the next step, an object was placed directly in the path between the signal source and the receiver. Data were collected for 30 seconds with and without the object in place.

The collected data were analyzed using the t-test to determine whether the data from the two scenarios show statistically significant differences. The significance level was set at 0.05. For the comparison of collected data, the T-statistic values indicate a significant difference between the groups, and the P-values suggest that the null hypothesis can be rejected. Therefore, there is a statistically considerable difference between the two groups, which implies that the presence of an object on the LOS link has a measurable effect on the observed power levels, significantly reducing them. The results from the example scenario in Experiment 4.2.1, with and without the object placed 0.3 m from the signal source, are as in table 5.1

Furthermore, the significance between the two scenarios at each distance can be visually observed through box plots and spectrograms.

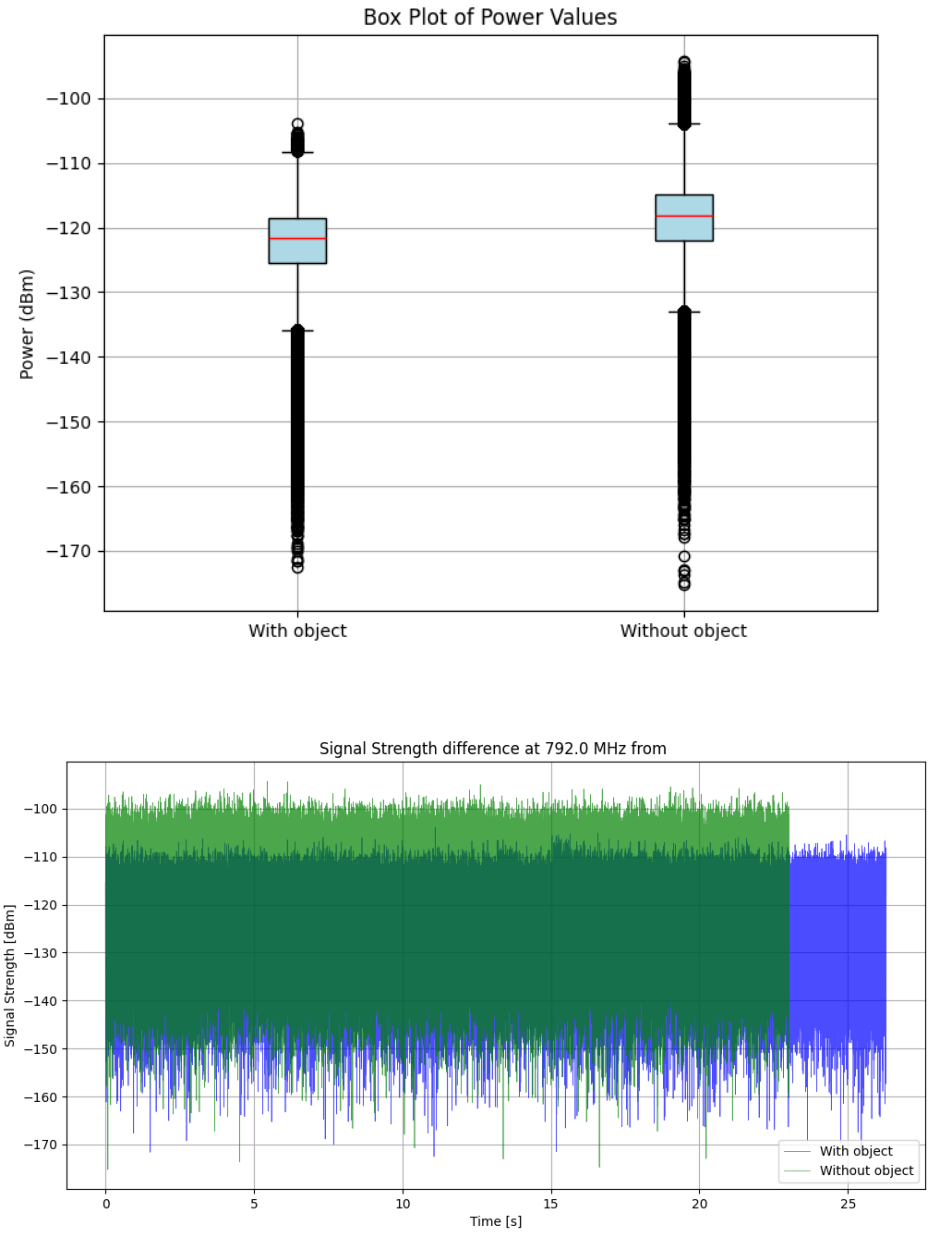

Figure 5.1: Difference of signal strength with and without the object when the signal receiver is at 0.6 m

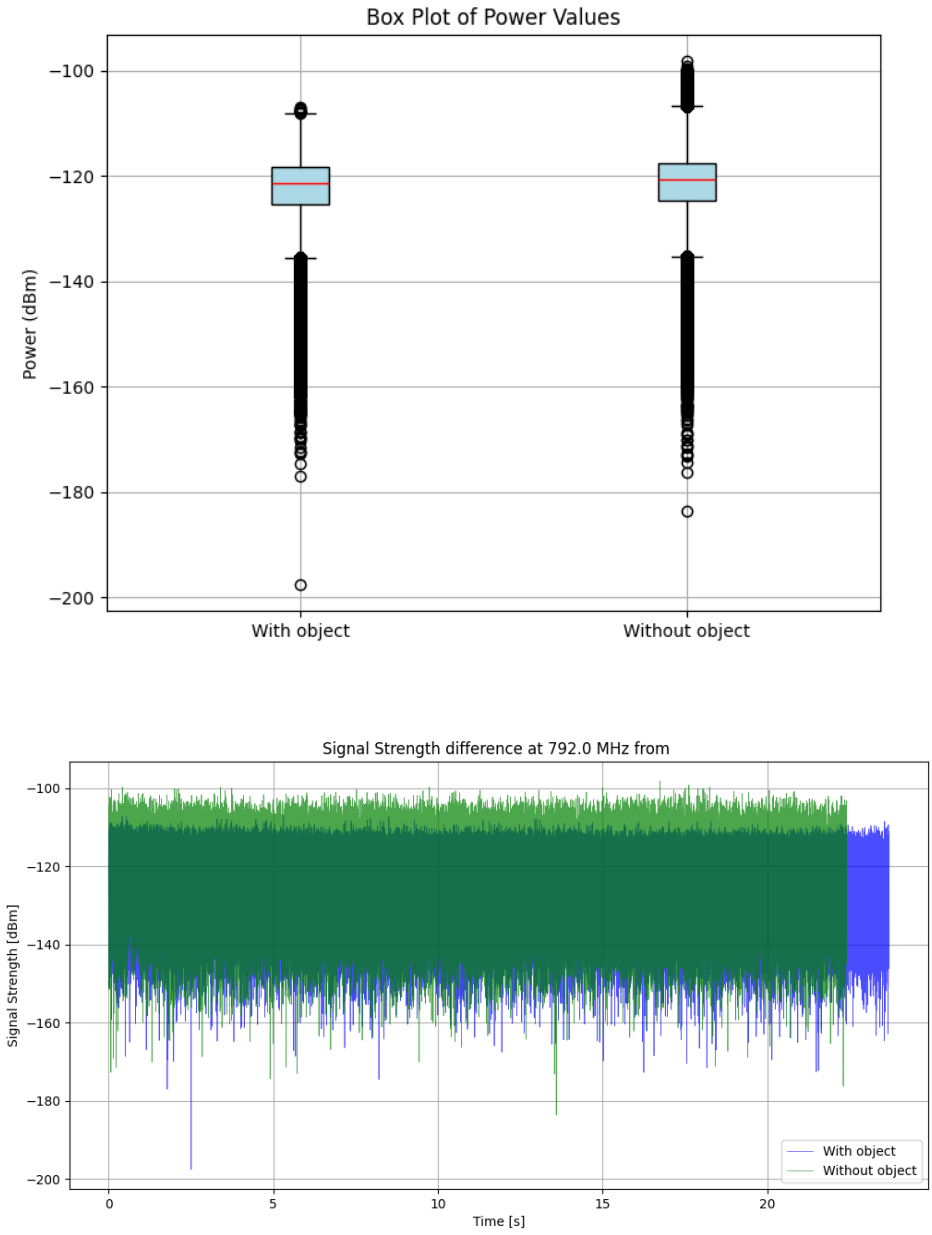

Figure 5.2: Difference of signal strength with and without the object when the signal receiver is at 2.7 m

To determine the most suitable representation of the signals, the mean, median, and mode were compared by calculating histograms to observe the distribution of the data (Figure 5.3 - Figure 5.8) which had skewness less than zero.

The histogram of power values indicates that the data distribution is not perfectly symmetric, making the choice of representation important.

The mean is a commonly used measure for continuous data, such as IQ data, and is

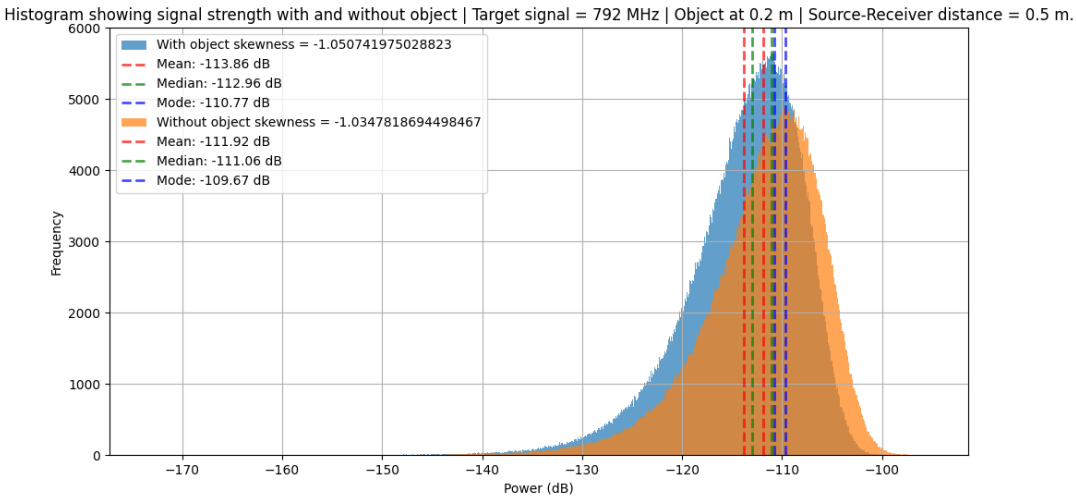

Figure 5.3: Histogram showing skewness with and without object in an outdoor open environment.— Target signal = 792 MHz — Object at 0.2 m — Source-Receiver distance = 0.6 m

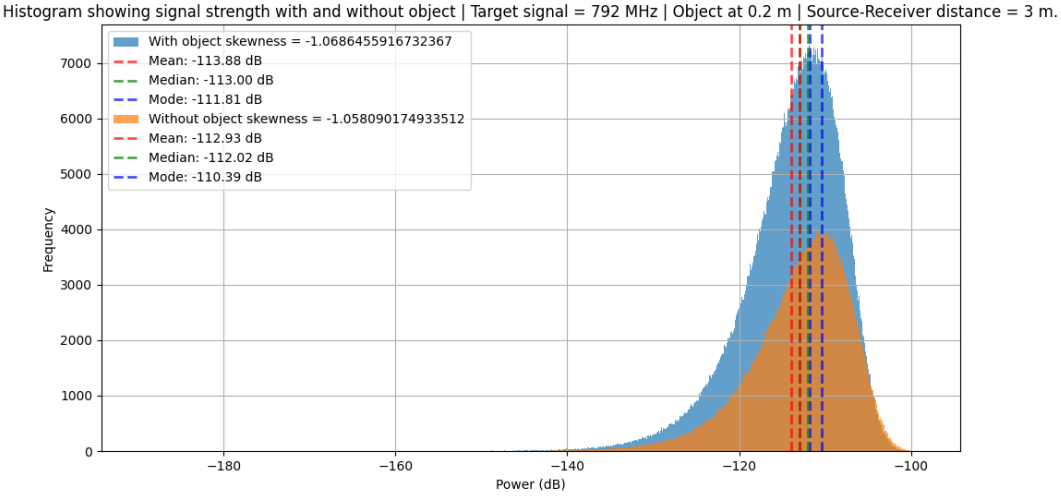

Figure 5.4: Histogram showing skewness with and without object in an outdoor open environment.— Target signal = 792 MHz — Object at 0.2 m — Source-Receiver distance = 3 m

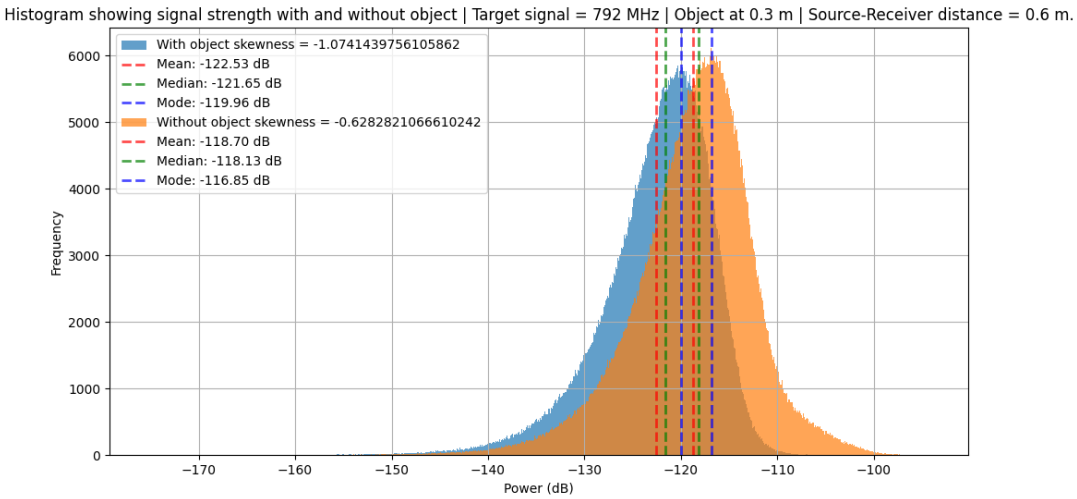

Figure 5.5: Histogram showing skewness with and without object in an indoor cluttered environment.— Target signal = 792 MHz — Object at 0.3 m — Source-Receiver distance = 0.6 m

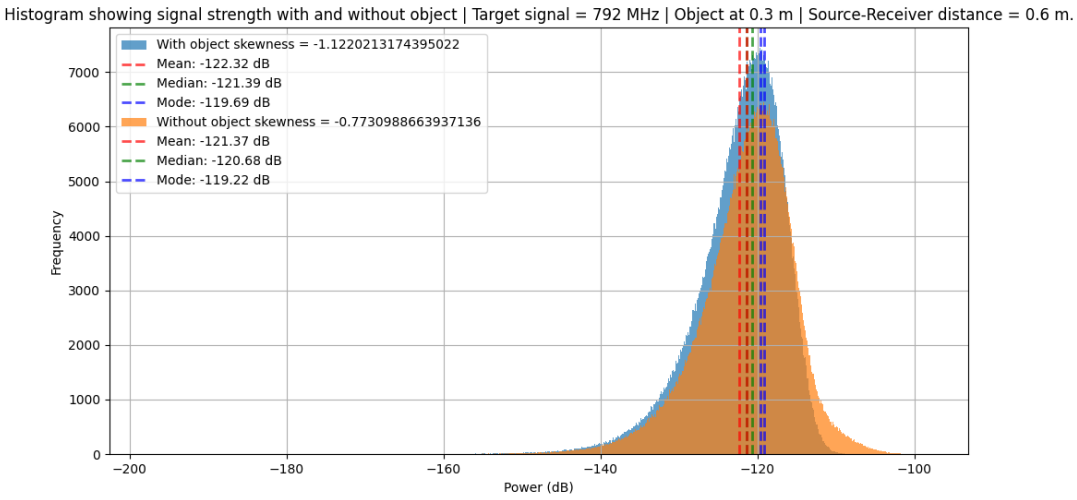

Figure 5.6: Histogram showing skewness with and without object in an indoor cluttered environment.— Target signal = 792 MHz — Object at 0.3 m — Source-Receiver distance = 2.7 m

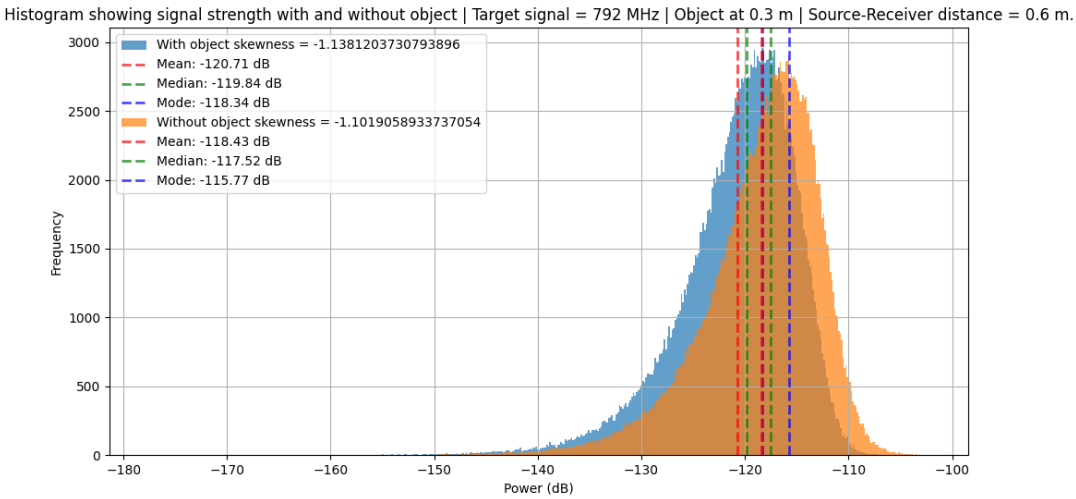

Figure 5.7: Histogram showing skewness with and without object in an indoor empty environment.— Target signal = 792 MHz — Object at 0.3 m — Source-Receiver distance = 0.6 m

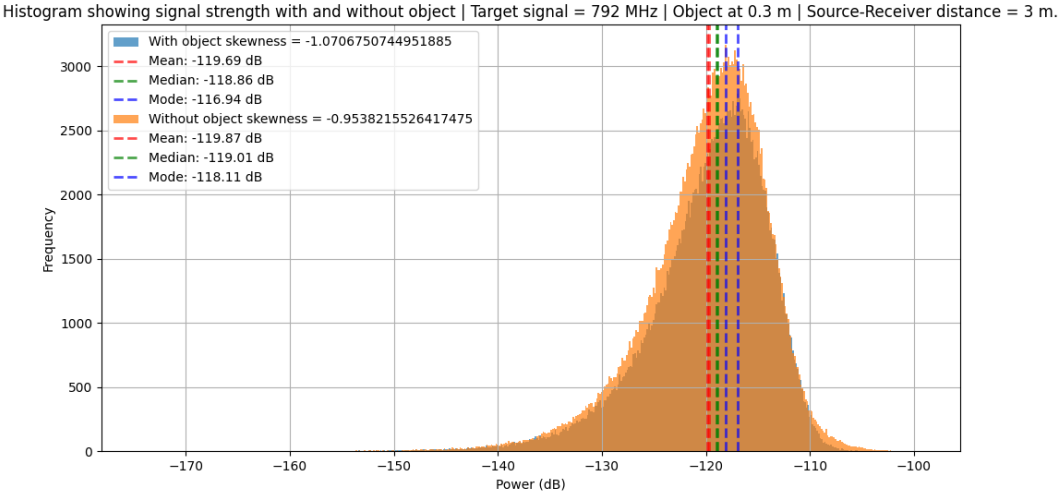

Figure 5.8: Histogram showing skewness with and without object in an indoor empty environment.— Target signal = 792 MHz — Object at 0.3 m — Source-Receiver distance = 3 m

effective when the data follows a normal distribution. However, it is highly sensitive to outliers, which can distort the representation when the data contains noise or anomalies as in data collected in this research. The mode is useful in identifying the most frequent values and is particularly effective in detecting dominant signal strengths in noisy environments. While it works well for categorical or discrete data, it may not provide the best representation for continuous data, especially when the data distribution varies.

The median, on the other hand, is a more robust measure of central tendency for skewed data. It is less affected by outliers compared to the mean while still providing a meaningful representation of the dataset. Since noise and outliers are expected in the data, the median serves as a stable choice that reflects the underlying trend without being overly influenced by extreme values.

Moreover, given that the mean, median, and mode exhibit nearly the same pattern across all instances (Figure 5.9a - Figure 5.9c), selecting the median ensures consistency while mitigating the impact of outliers. Thus, the median is chosen as the representative measure for the later analyses.

A higher RSS is expected in the scenario without an obstruction, as the absence of an object eliminates the shadowing effect. The experiment conducted in the outdoor ground environment demonstrates the expected behavior up to a distance of 3 m (Figure (5.10a)) decreasing the signal from 0.98 to 1.9 dBm. Similarly, in the indoor empty environment, the signal dropping pattern is visible up to 3.6 m varying from 0.65 to 2.32 dBm, consistent with the expected propagation pattern in a relatively uncluttered space (Figure (5.11a)). However, in the indoor working environment, the signal is only detectable up to 2.4 m, which is a result of the physical limitations of the available space, including obstacles that introduce additional interference and signal attenuation (Figure (5.12a). But the signal drop is between 0.71 and 3.52 dBm. An interesting observation is that the graphs obtained for indoor working environment has a smoother propagation pattern with distance. This can be due to limited external noise signal filtered through concrete walls in to the area under observation compared to other environments.

Another method to determine the maximum detectable distance is by analyzing the

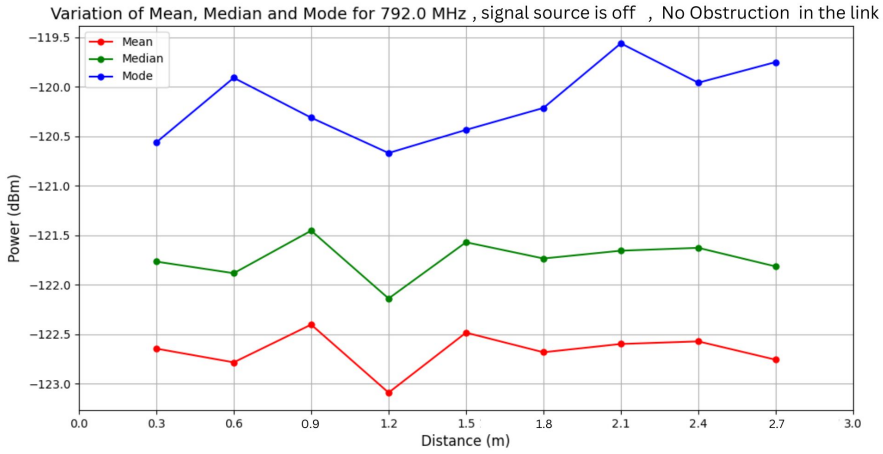

(a)

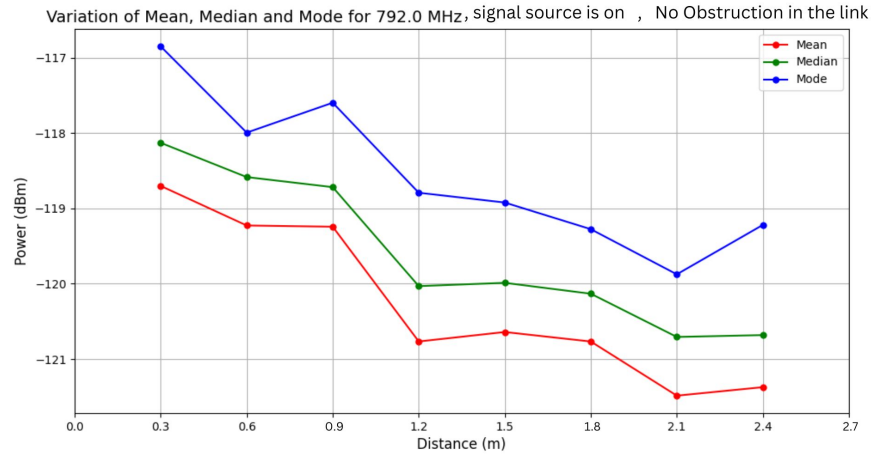

(b)

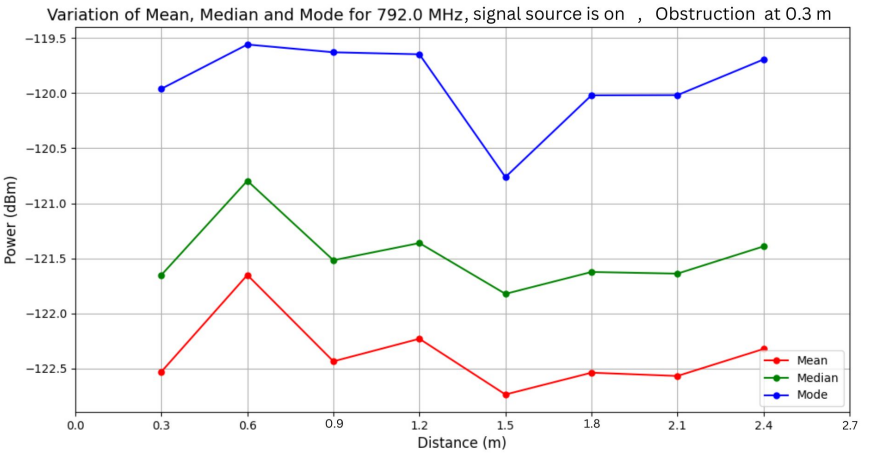

(c)

Figure 5.9: Variation of mean, median, and mode for three scenarios in the indoor working environment. (a) RSS when the signal source is off (b) Signal source operating without any obstruction. (c) Signal source with an object placed between the source and receiver at 0.3 m distance.

SNR. SNR value between the signal without object and signal with object would indicate the significance of the signal going through the object compared to the free path signal [1]. The maximum detection distance would be when the SNR value is closest to the zero before the multipath effects, meaning the signal change induced by the object is no longer distinguishable.

There are several methods to calculate the SNR value. The mean to standard deviation method to calculate SNR is suitable in cases where the signal occurs randomly or when the frequency components are unknown with the assumption that the noise is gaussian. But in this case the target frequency is known and noise can be measured as a single signal. Therefore, the power ratio method is used.

Use SNR to Measure Object Interference

$$SNR = 10 \cdot \log_{10} \left(\frac{P_{\text{signal without object}}}{P_{\text{with object}}} \right)$$

- If SNR is large, the object significantly reduces the signal quality.
- If SNR is small, the object has little impact on the signal.
- If SNR drops below 0, the noise dominates the signal and the object is no longer detectable.

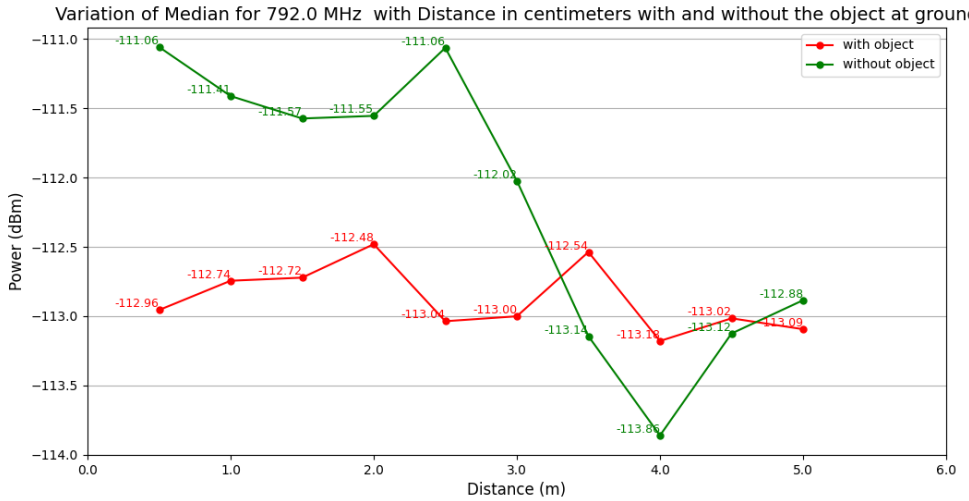

(a)

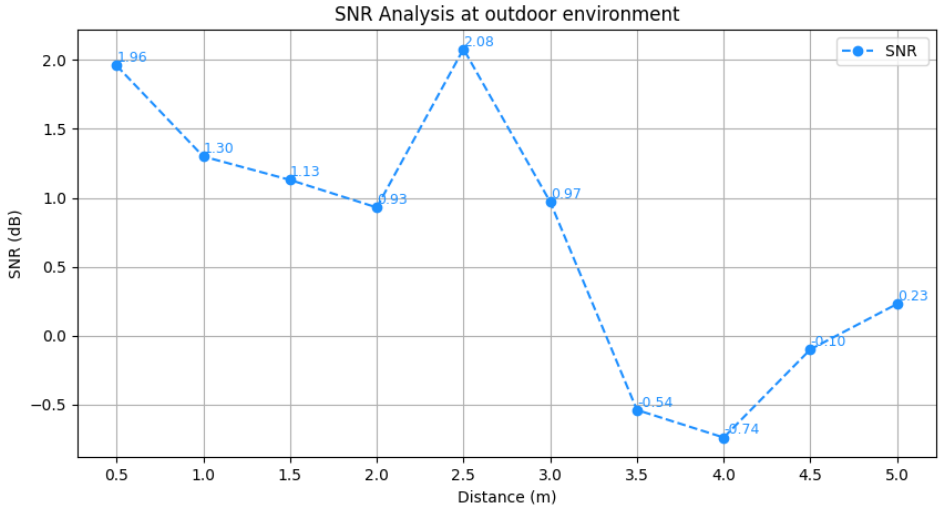

(b)

Figure 5.10: Outdoor ground environment (a) Results of data collection (b) Signal to Noise Ratio analysis

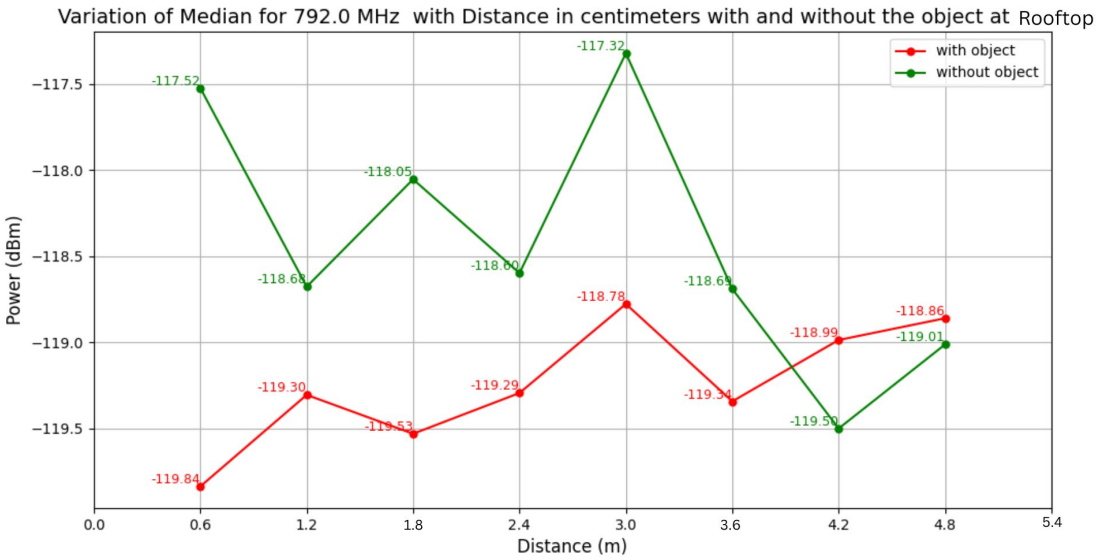

(a)

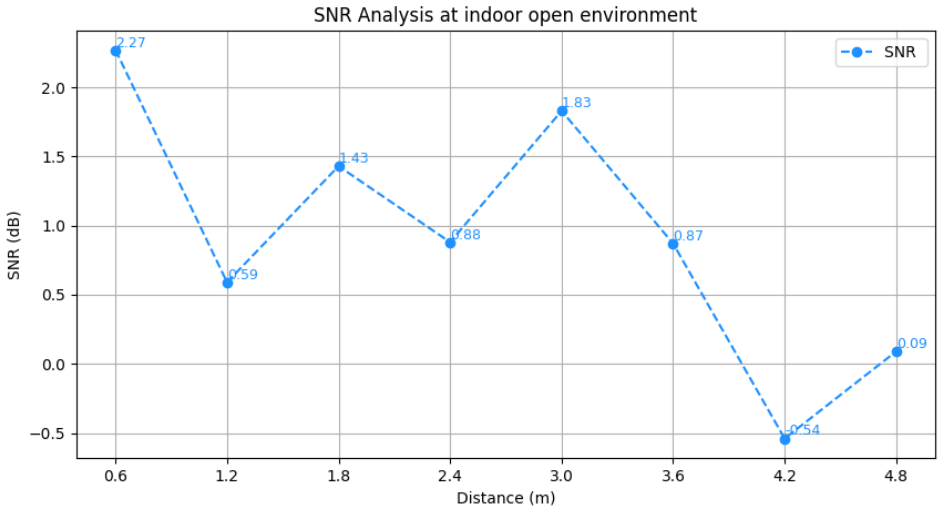

(b)

Figure 5.11: Indoor open environment (a) Results of data collection (b) Signal to Noise Ratio analysis

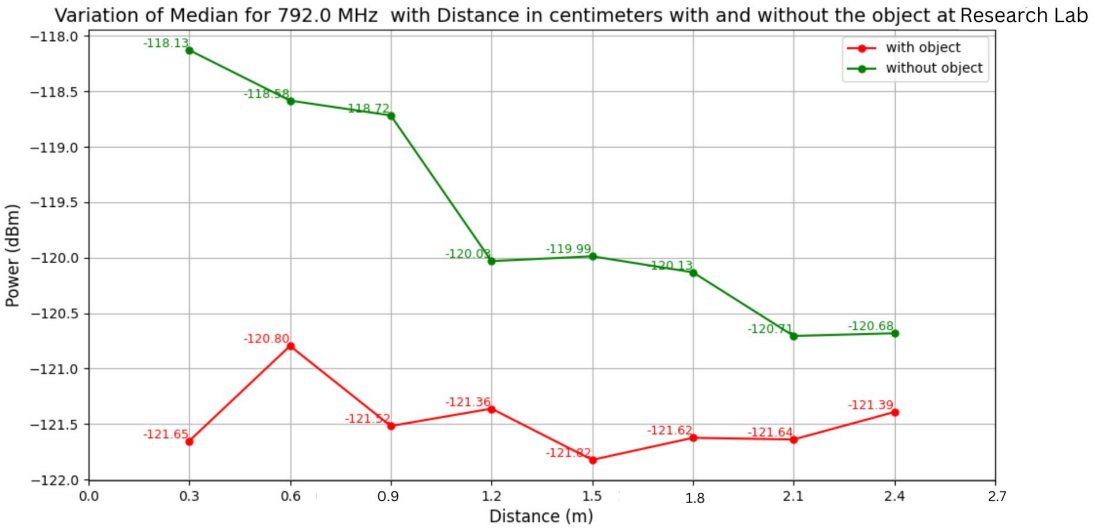

(a)

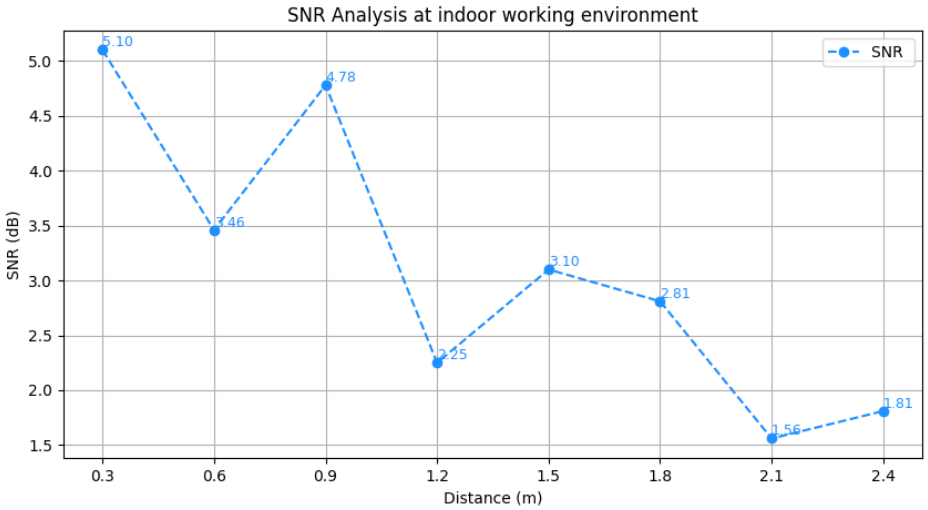

(b)

Figure 5.12: Indoor working environment (a) Results of data collection (b) Signal to Noise Ratio (SNR) analysis

In the outdoor ground environment, the smallest SNR that remains above zero, before noise dominates the signal, is recorded at a distance of 3 m from the signal source. Beyond this point, detection becomes unreliable due to the uncertainty in SNR (Figure 5.10b). Indoor open environment demonstrate a positive SNR value until 3.6 m from the signal source (5.11b). For the scenario in the indoor working environment the smallest SNR above zero before noise dominate the signal is recorded at the distance of 2.4 m from the signal source (Figure 5.12b). The study concludes that the maximum distance

to detect an object vary based on the environment.

Another key factor influencing RSS, in addition to noise, is the CPU workload. As previously explained, the CPU workload affects the power consumption of the circuit. Which influences the strength of the emitted EM radiation. Therefore, the signal strength of the EM radiation was observed by incrementally increasing the CPU workload by 10% at each step, and plotted the corresponding PSD plots (Figure 4.4).

The results confirm that the EM radiation corresponding to different CPU workloads can be distinguished from each other. However, further analysis reveals that for any given CPU workload, the signal strength is significantly reduced when an object is placed in the direct line of sight between the signal source and the receiver (Table 5.2).

Above experiments lead to identify three main factors affecting RSS as,

- Transmitted signal strength (This depends on CPU workload)
- Location of the object in the direct signal path
- The distance between the signal receiver and the signal source.

The fundamental requirement for a tomographic setup is the ability to detect the presence of an object crossing a single link between the signal source and the signal receiver. Next experiments were designed to investigate the effects of an object on this link. Experiment 4.4.1 examines how the presence of an object affects the signal strength along the link as the distance between the source and receiver increases, when the transmitted signal strength and the location of the object kept constant. On the other hand experiment 4.4.2 explores the impact of a moving object on a single link, where the transmitted signal strength and the distance between the receiver and the source are maintained static.

According to the circular coverage model of EM radiation propagation, the RSS typically decreases with distance following an inverse proportionality of $1/d^n$. The graph in Figure 5.13 which represents the signal emitted by the source operating at a static workload and captured at 792 MHz, shows a decline in RSS consistent with this theoretical model. In contrast, the graph when the desktop is turned off indicates

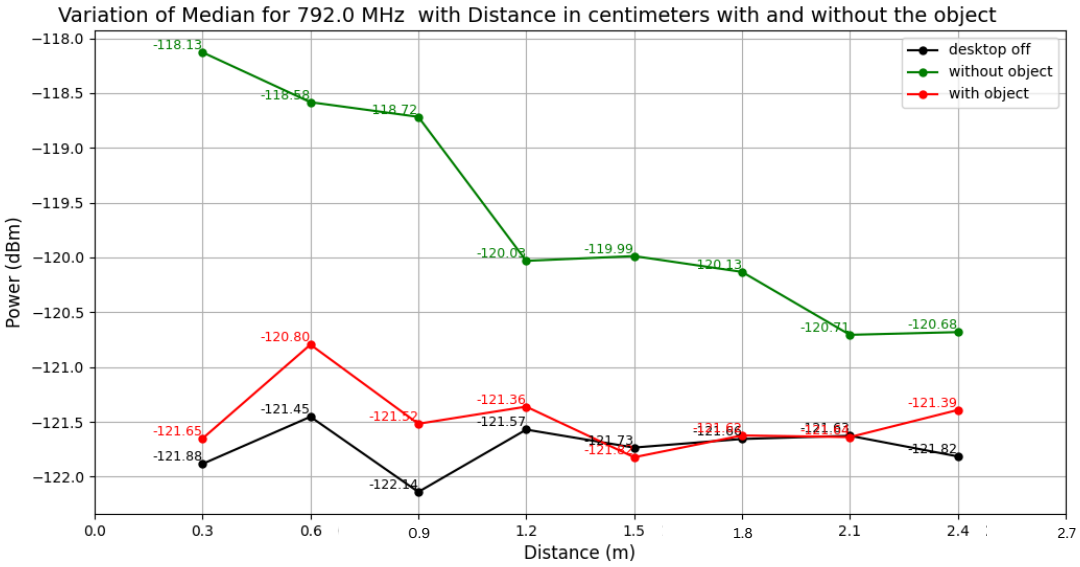

Figure 5.13: Variation of median signal strength at 792 MHz with distance when the object is stationary 0.3 m from the receiver.

the RSS of ambient noise at each position of the receiver. The ambient noise remains nearly constant across varying distances and is consistently lower than the signal strength captured when the signal source is active.

The effect of an object on the RSS is clearly visible in the Figure 5.13 where the object is stationary at a distance of 0.3 m from the receiver. At shorter distances, the difference in RSS is more pronounced. Indicating that the ability to detect the object diminishes as the distance between the receiver and the signal source increases. Since the object is placed relatively close (0.3 m) to the signal source, a greater proportion of the signal paths are blocked. This lead to a significant reduction in RSS which approaches the ambient noise level at each position. This phenomenon is caused by the shadowing effect in which the object obstructs the propagation of the signal. The results suggest that in the indoor working environment, the presence of the object remains detectable up to a distance of 2.7 m from the signal source.

Experiment 4.4.2 further investigates the impact of placing the object at different positions along the link while keeping the distance between the signal source and the receiver constant. The findings indicate that the shadowing effect on RSS is most significant when the object is placed closer to either the signal source or the receiver.

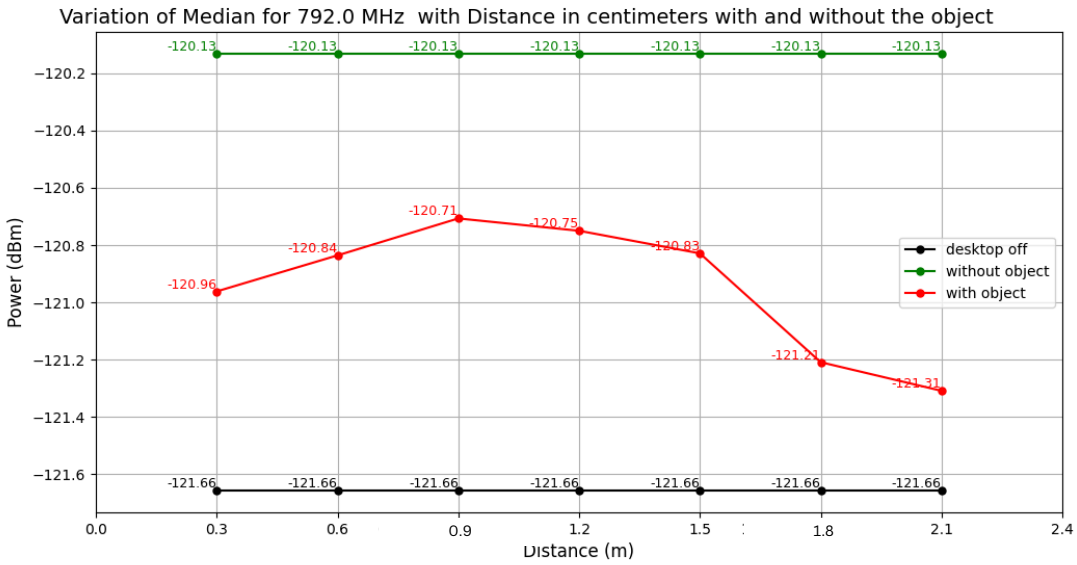

Figure 5.14: Variation in the median RSS at 792 MHz with distance, as the object moves toward the receiver.

Conversely, the drop in RSS due to shadowing is minimal when the object is positioned near the center of the link. This observation leads to the identification of two regions along the link: a high-impact area, where the object significantly affects the signal, and a low-impact area, where the effect is less pronounced (Figure 5.15).

For the data collected in the indoor working environment calculated SNR is as in Figure 5.16. One method of distinguishing between high impact and area and low impact area is by considering a threshold as follows,

$$\text{SNR}_{Threshold} = \frac{\text{SNR}_{Max} + \text{SNR}_{Min}}{2} \tag{5.1}$$

The necessity to distinguish distance based on SNR and requirement to divide the area into two is considered when designing the Eq. 5.1.

Based on the experimental results, the threshold value is determined as follows:

$$\frac{(2.31 + 1.40)}{2} = \frac{3.71}{2} = 1.855$$

Based on this threshold, the distances corresponding to high-impact and low-impact areas are identified as follows (Figure 5.16):

high impact and area : 0-0.55 m and 1.69-2.1 m

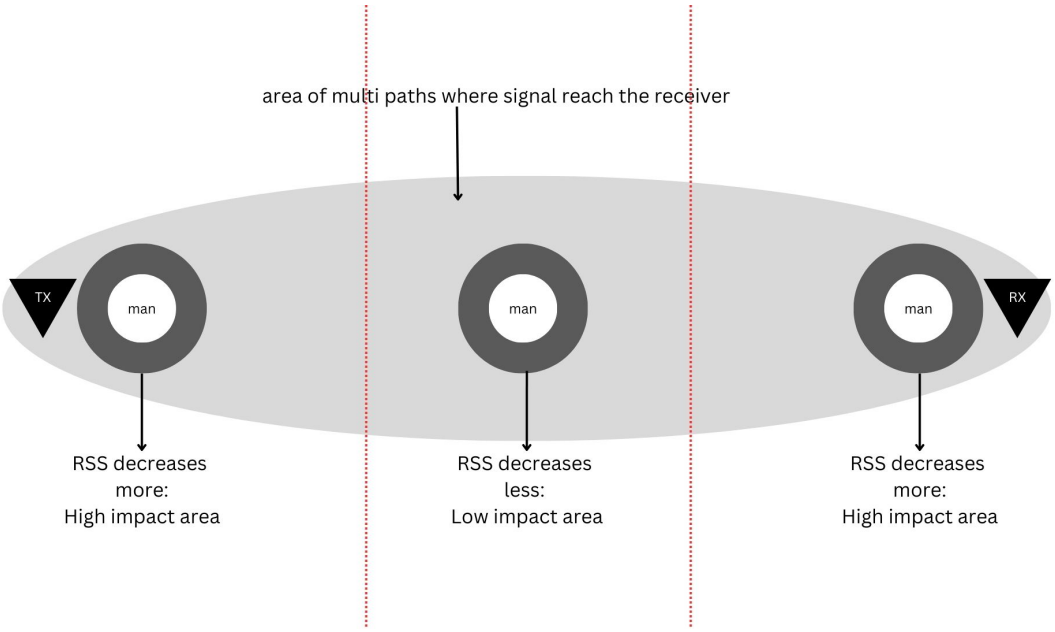

Figure 5.15: Illustration of multi path effects and their impact on signal propagation in the link.

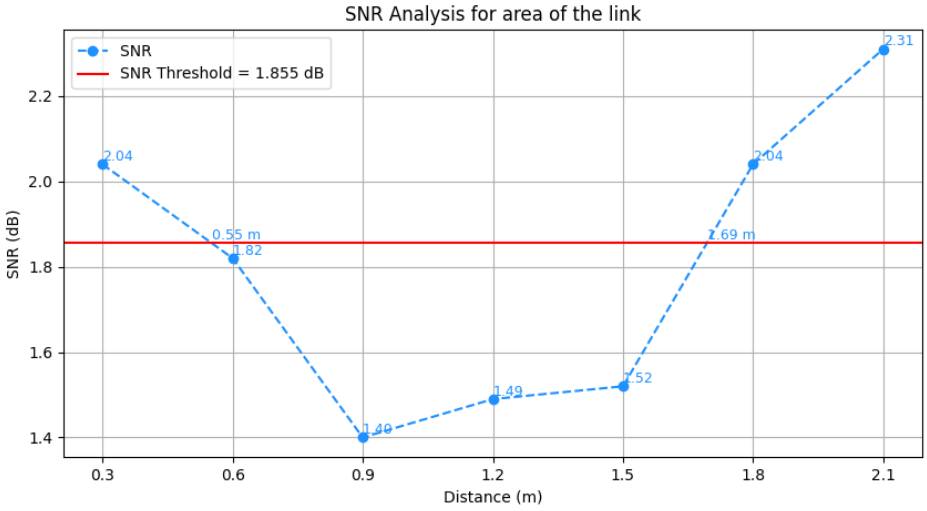

Figure 5.16: Threshold determination using SNR analysis

low impact areas :0.55 m to 1.69 m

This research proposes the potential use of the above observation to implement refined weighting method in tomographic systems. Such a method could reduce algorithmic complexity and enhance the power efficiency of the setup.

The derived information can be further interpreted to obtain following equations to model the shadowing effect by the object on the single link at a specific distance from the signal source.

$$P_{\text{received}} = P_{\text{transmitted}} - \text{Path Loss} - \text{Static Loss} \tag{5.2}$$

$$P'_{\text{received}} = P_{\text{transmitted}} - \text{Path Loss} - \text{Static Loss} - \text{Shadowing Loss} \tag{5.3}$$

$$P_{\text{received}} - P'_{\text{received}} = \text{Shadowing Loss} \tag{5.4}$$

Let P_{received} represent the RSS in the absence of any object interference and let P'_{received} be the RSS with and interference of an object. When we consider the effect of internal and external noise as static for a given scenario the shadowing effect of the object on the link can be derived by the difference of P_{received} and P'_{received} using the Eq. 5.4.

Knowing this can make it easier to build better models and improve signal processing in places where objects can cause interference.

5.1 Algorithm to Approximate Position in a Single Link

In this research, the exact position of a person located along a single link cannot be uniquely determined due to the near-symmetry observed in the graph shown in Figure 5.14. However, based on the RSS at a given moment, two possible positions can be estimated. When one of these positions corresponds to the actual location, the estimation achieves a mean absolute error of 0.1072 m. By incorporating tracking techniques such as the Kalman filter, the accuracy of localization can be further improved.

The nearly symmetric graph observed resembles the shape of a quadratic function, which can be estimated by identifying the vertex and two additional data points. In this context, the maximum RSS value is recorded when the person is positioned at the center

of the link, while minimum RSS values are observed when the person is near either the transmitter or the receiver. This behavior enables a straightforward calibration process: The parameters of the polynomial model can be determined by placing the person at the center and near the nodes and recording the corresponding RSS values. Once the polynomial model is established, it can be used in reverse. The corresponding positions can be estimated by solving the quadratic equation as an inverse problem when given an observed RSS value.

Input data

Table 5.3: RSS Measurements at Selected Distances

Actual Distance (m)	RSS (dBm)
0.3	-12096152978.51
1.2	-12074991571.14
2.1	-12130834859.59

Polynomial model

$$\text{Signal Strength} = -47{,}533{,}762.8548 \cdot d^2 + 94{,}813{,}319.1427 \cdot d - 12{,}120{,}318{,}935.5978 \quad (5.5)$$

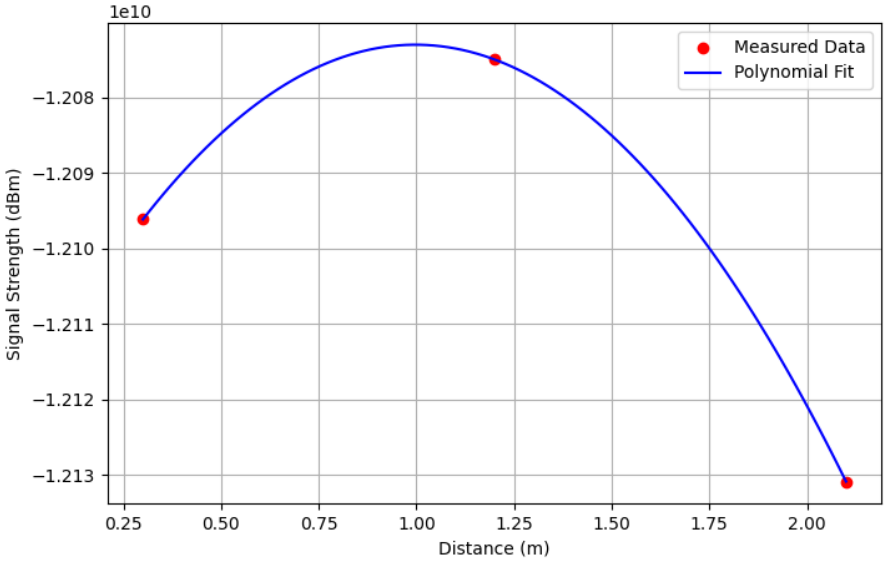

Figure 5.17: Graph of the polynomial model

The obtained polynomial model gives 0.1072 m mean absolute error. The minimum mean absolute error is obtained when considered the vertex and two minimum RSS values to build the polynomial model.

Estimations from the model

Table 5.4: Estimated Distances from the Polynomial Model

RSS (dBm)	Estimations (m)	Actual distance (m)	Deviation of the closest estimation (m))
-120.83582614982215	0.5264 , 1.4683	0.6	0.0736
-120.82876139915794	0.5424 , 1.4522	1.5	0.0478
-121.20854944402521	-0.0056 , 2.0003	1.8	0.2003

Algorithm 1 Estimate Distance from Signal Strength

Require: Signal strengths $S = [s_1, s_2, \ldots, s_n]$, Distances $D = [d_1, d_2, \ldots, d_n]$
Require: New signal strength S_{new}, Reference value s_{ref} (This quadric coefficient c), Quadratic coefficients a, b
Ensure: Estimated distance(s) corresponding to S_{new}
1: **Step 1: Fit Polynomial Model**
2: Use polynomial regression (degree = 2) to fit model to S and D:

$$s = ad^2 + bd + c$$

3: Extract coefficients a, b, c
4: **Step 2: Estimate Distance from S_{new}**
5: Form shifted polynomial:

$$f(d) = ad^2 + bd + (c - S_{\text{new}})$$

6: Solve $f(d) = 0$ for d
7: Filter real, positive roots as valid distances
8: Output estimated distances =0

According to the algorithm, each RSS measurement provides two estimates of possible positions due to the symmetry of the signal curve. However, by using multiple RSS measurements over time, we can track the movement and filter out uncertainty with applying the Kalman filter for a stationary or moving person along a single link.

The Kalman Filter helps by combining:

- Current measurement (RSS-based position estimate)
- Previous position estimate (prediction based on motion model)

The filter smooths out noisy measurements, favors consistent trajectories, and eliminates physically impossible jumps between the two possible solutions at each time step. Over time, the Kalman filter helps the system lock onto the true position, improving the accuracy of localization compared to what a single RSS reading provide.

5.2 Theoretical Model to Obtain a Tomographic Image

This research results in discovering the impact of an object on a single link made by a signal source of unintentional EM side channel and a signal receiver. In this study, a single frequency harmonic (792 MHz) of the emitted radiation and a single link quality parameter, namely the RSS, have been evaluated.

Building on this knowledge, two methods emerge for creating a tomographic image that localizes an object:

1. Utilizing a single link quality parameter with multiple links.
2. Employing multiple link quality parameters with one or more links.

The first method, which leverages a single link quality parameter across multiple links, was proposed by Wilson and Patwari (Wilson & Patwari 2010). This approach, outlined below can be adapted for the purpose of tomography using multiple links of unintentional EM radiation as well.

Tomographic Imaging Model by Wilson and Patwari

The RSS can be expressed as:

$$y_i(t) = P_i - L_i - S_i(t) - F_i(t) - \nu_i(t)$$

where:

- P_i is the transmitted power in dB.
- $S_i(t)$ is the shadowing loss in dB due to objects that attenuate the signal.
- $F_i(t)$ is the fading loss in dB caused by constructive and destructive interference in a multi path environment.
- L_i represents static losses in dB due to distance, antenna patterns, and device inconsistencies.
- $\nu_i(t)$ is the measurement noise.

The shadowing loss $S_i(t)$ for a given link (Figure 5.18) can be approximated as the sum of attenuation occurring in each voxel, weighted differently for each link:

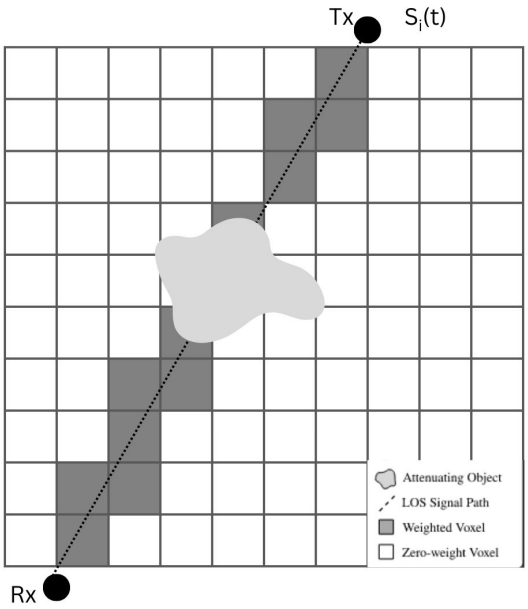

Figure 5.18: An RTI network link of a direct LOS path, with shadowing of an object indicated by darkened voxels

$$S_i(t) = \sum_{j=1}^{N} w_{ij} x_j(t)$$

where:

- $x_j(t)$ is the attenuation in voxel j at time t.
- w_{ij} is the weighting factor that determines the contribution of voxel j to link i.

To determine the weighting for each link in the network, an ellipsoid with foci at the node locations is used. The weighting factor w_{ij} for voxel j in link i is defined as:

$$w_{ij} = \frac{1}{\sqrt{d}} \begin{cases} 1, & \text{if } d_{ij}(1) + d_{ij}(2) < d + \lambda \\ 0, & \text{otherwise} \end{cases} \tag{5.6}$$

where:

- d is the distance between the two nodes.
- $d_{ij}(1)$ and $d_{ij}(2)$ are the distances from the center of voxel j to each node in link i.

- λ is a tunable parameter controlling the ellipse width.

This method assigns nonzero weights to voxels within a specified region around the link path and a voxel outside the signal path has $w_{ij} = 0$, removing it from the final calculations.

Change in Received Signal Strength (RSS)

To simplify the analysis, we consider only the change in RSS over time, removing static losses:

$$\Delta y_i = y_i(t_b) - y_i(t_a) = S_i(t_b) - S_i(t_a) + F_i(t_b) - F_i(t_a) + \nu_i(t_b) - \nu_i(t_a)$$

Rewriting in terms of voxel attenuation change:

$$\Delta y_i = \sum_{j=1}^{N} w_{ij} \Delta x_j + n_i$$

where:

- $\Delta x_j = x_j(t_b) - x_j(t_a)$ represents the attenuation change in voxel j.
- $n_i = F_i(t_b) - F_i(t_a) + \nu_i(t_b) - \nu_i(t_a)$ is the combined fading and measurement noise.

Matrix Representation

For an entire network, the system of equations can be written in matrix form:

$$\Delta y = W \Delta x + n \tag{5.7}$$

where:

$$\Delta y = [\Delta y_1, \Delta y_2, ..., \Delta y_M]^T \quad \text{(Vector of RSS differences)}$$

$$\Delta x = [\Delta x_1, \Delta x_2, ..., \Delta x_N]^T \quad \text{(Vector of voxel attenuation changes)}$$

$$n = [n_1, n_2, ..., n_M]^T \quad \text{(Noise vector)}$$

$$W_{i,j} = w_{ij} \quad \text{(Weighting matrix of size } M \times N\text{)}$$

Here, M is the number of links, and N is the number of voxels. The goal in RF tomography is to estimate Δx, the attenuation image, given the measurements Δy and the known weighting matrix W.

Adjustment to the Algorithm

Based on the linear model proposed by Patwari and Wilson Eq. (5.7), several methods can be employed to reduce computational cost:

1. Reduce the dimensionality of the matrices to limit unnecessary computations.
2. Make the weight matrix sparse to improve computational efficiency.

Considering the impact of an object's location on different links, a modified weighting model is proposed. This model dynamically adjusts the weight matrix based on the observed changes in RSS, Δy. The proposed method suggests to focus on fewer number of attenuated voxels as in Figure 5.19 instead of focusing on all the voxels in the link as in Figure 5.18.

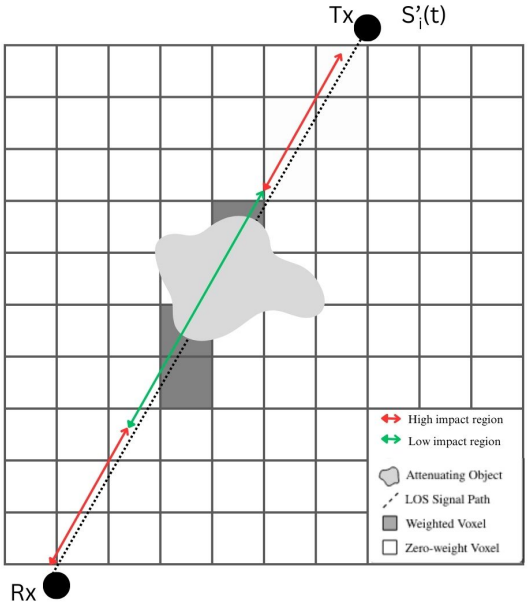

Figure 5.19: An RTI network link of a direct LOS path, with shadowing of an object indicated by darkened voxels of only the impacted area based on the threshold

$$w_{high_{ij}} = \frac{1}{\sqrt{d}} \begin{cases} 1, & \text{if } d_{ij}(1) + d_{ij}(2) < d + \lambda \text{and if } \Delta y > Threshold\Delta y \\ 0, & \text{otherwise} \end{cases} \tag{5.8}$$

$$w_{low_{ij}} = \frac{1}{\sqrt{d}} \begin{cases} 1, & \text{if } d_{ij}(1) + d_{ij}(2) < d + \lambda \text{and if } \Delta y \leq Threshold\Delta y \\ 0, & \text{otherwise} \end{cases} \tag{5.9}$$

where:

d is the distance between the two nodes.

$d_{ij}(1)$ and $d_{ij}(2)$ represent the distances from the center of voxel to the two node locations for link .

λ is a tunable parameter describing the width of the ellipse.

$Threshold\Delta y$ is a calibrated threshold for distinguishing between high and low attenuation impacts.

The $Threshold\Delta y$ is determined based on the maximum and minimum impact an object can have on a link. This threshold can be set during a calibration phase by considering variations due to object placement and link length.

For each link i, we obtain two potential weighting matrices: w_{high_i} and w_{low_i}. The final weight matrix W is constructed based on the following selection criteria:

$$W_i = \begin{cases} w_{low_i}, & \text{if } \Delta y_i < \text{Threshold } \Delta y \\ w_{high_i}, & \text{if } \Delta y_i > \text{Threshold } \Delta y \text{ and Threshold } \Delta y \neq 0 \\ 0, & \text{if Threshold } \Delta y = 0 \end{cases} \tag{5.10}$$

Once the global MxN weight matrix is constructed, standard RTI computations can proceed using Eq. (5.7):

Computational Cost and Time Complexity

To analyze the computational complexity of both the traditional and proposed methods, we break down the cost into three main components:

(1) the cost of creating the weight matrix

(2) the cost of selecting weight matrices based on Δy

(3) the cost of matrix multiplication.

1. Cost of Creating the Weight Matrix

Algorithm 2 Construct Weight Matrix W and Estimate Δx in RF Tomography

Require: Measured RSS changes $\Delta y = [\Delta y_1, \ldots, \Delta y_M]^T$
Require: Node pair distances d_i, voxel distances $d_{ij}(1), d_{ij}(2)$ for all links i and voxels j
Require: Threshold value ThresholdΔy, tunable parameter λ
Ensure: Estimated attenuation image Δx

Initialize empty weight matrix $W \in \mathbb{R}^{M \times N}$
for each link $i = 1$ to M **do**
  for each voxel $j = 1$ to N **do**
    Compute total voxel distance: $d_{ij}^{\text{sum}} = d_{ij}(1) + d_{ij}(2)$
    if $d_{ij}^{\text{sum}} < d_i + \lambda$ **then**
      if $\Delta y_i >$ ThresholdΔy **then**
        Set $w_{ij}^{\text{high}} = \frac{1}{\sqrt{d_i}}$
      else
        Set $w_{ij}^{\text{low}} = \frac{1}{\sqrt{d_i}}$
      end if
    else
      Set $w_{ij}^{\text{high}} = 0$, $w_{ij}^{\text{low}} = 0$
    end if
  end for
  if Threshold$\Delta y = 0$ **then**
    Set $W_i = \mathbf{0}$ (zero row)
  else if $\Delta y_i >$ ThresholdΔy **then**
    Set $W_i = w_i^{\text{high}}$
  else
    Set $W_i = w_i^{\text{low}}$
  end if
end for
Solve the system $\Delta y = W \Delta x + n$ for Δx using regularized least squares or another RTI method
return Estimated attenuation image Δx =0

For the traditional method, the weight matrix W is computed using Eq. (5.6), which requires iterating over all voxels N for each link M, leading to a computational complexity of:

$$O(MN)$$

In the proposed method, two weight matrices, w_{high} and w_{low}, are constructed separately by iterating over all N voxels for each of the M links twice. This results in a computational complexity of:

$$O(2MN)$$

2. Cost of Combining the Weight Matrices

In the proposed method, the final weight matrix W is dynamically determined based on the observed Δy values using the selection criteria in Eq. (5.10). This requires iterating over all M links to check Δy and selecting the appropriate weight matrix (w_{low} or w_{high}). This operation incurs an additional cost of:

$$O(M)$$

The traditional method does not require this step, therefore its cost remains $O(1)$ for this component.

3. Cost of Matrix Multiplication

For both methods, the computational cost of matrix multiplication depends on the sparsity of the weight matrix W:

If W is dense, the multiplication $W\Delta x$ requires $O(MN)$ operations.

If W is sparse, we can optimize the multiplication by only computing values where $W_{ij} \neq 0$, reducing operations to $O(kN)$, where k is the average number of nonzero elements per row.

Thus, for the traditional method, the matrix multiplication cost is:

$$O(MN)$$

For the proposed method, since the weight matrix is dynamically constructed based on Δy, it benefits from increased sparsity, leading to multiplication cost of:

$$O(kN)$$

Total Computational Cost Comparison

The total computational cost for the **iterative steps** of each method is summarized as follows:

Traditional Method:

Cost of matrix multiplication $= O(MN)$

Proposed Method:

Cost of creating global weight matrix + Cost of matrix multiplication $= O(M) + O(kN)$

Both methods remain $O(MN)$ in the worst case. However, the proposed method benefits from sparsity, reducing the cost of matrix multiplication from $O(MN)$ to $O(kN)$, which can lead to significant performance improvements when $k \ll M$.

5.3 Evaluation

The primary objective of this research is to evaluate the accuracy of tomographic techniques that utilize unintentional EM radiation emitted by computing devices. The results demonstrate that, using a single transmission link and a single signal parameter, it is possible to estimate two potential object locations within the LOS, achieving a mean absolute error of approximately 0.1072 m.

An additional contribution of this study is the development of an improved algorithm that significantly reduces computational complexity from $O(MN)$ to O$(M) + O(kN)$ where $k \ll M$, enhancing the feasibility of real-time processing in practical deployments but with the cost of more complicated calibration phase. Also in comparison suggested method has a $O(2MN)$ to initialize the weights matrices while the original algorithm has $O(MN)$ computational cost.

In this research, 792 MHz was used as the target frequency, and RSS was the key link quality metric observed. The presence of a person introduced detectable RSS changes ranging from 0.65 to 3.52 dBm. These signal disturbances were measurable up to 2.4 m in cluttered indoor environments and up to 3 m in open outdoor spaces. Prior studies in this signal range are not recorded to be compared with these values but prior studies using 2.4 GHz frequencies reported RSS reductions of 2 to 5 dBm at a 2 m distance, with greater signal degradation observed over shorter links (Table 2.2).

Table 5.1: Statistical Values and T-Test Results for varying distances

Distance (T_x-R_x)	**Mean (NLoS) [dBm]**	**Mean (LoS) [dBm]**	**Std (NLoS) [dBm]**	**Std (LoS) [dBm]**	**Variance (NLoS)**	**Variance (LoS)**	**T-Statistic**	**P-Value**	**Conclusion**
0.6 m	-122.5310	-118.7008	5.6615	6.1924	32.0524	38.3457	-448.3346	0.0	Significant difference
0.9 m	-121.6517	-119.2265	5.7355	6.1457	32.8965	37.7695	-284.4416	0.0	Significant difference
1.2 m	-122.4362	-119.2429	5.6094	6.2806	31.4657	39.4463	-387.3412	0.0	Significant difference
1.5 m	-122.2310	-120.7661	5.5987	5.9547	31.3451	35.4587	-179.4291	0.0	Significant difference
1.8 m	-122.7374	-120.6408	5.5812	6.0213	31.1499	36.2556	-250.7560	0.0	Significant difference
2.1 m	-122.5392	-120.7666	5.5859	6.0467	31.2019	36.5622	-210.3909	0.0	Significant difference
2.4 m	-122.5691	-121.4854	5.6052	5.8240	31.4186	33.9195	-126.2256	0.0	Significant difference
2.7 m	-122.3238	-121.3728	5.6077	5.9768	31.4462	35.7225	-110.1515	0.0	Significant difference

Table 5.2: Statistical Values and T-Test Results for varying CPU workloads

CPU workload (%))	Median (NLoS) [dBm]	Median (LoS) [dBm]	T-Statistic	P-Value	Conclusion
10	-121.76	-121.04	-93.5986	0.00	Significant difference
20	-121.79	-121.04	-101.9562	0.00	Significant difference
30	-121.64	-120.69	-134.0214	0.00	Significant difference
40	-121.28	-120.45	-106.7482	0.00	Significant difference
50	-121.39	-120.31	-140.7272	0.00	Significant difference
60	-121.44	-120.33	-152.6532	0.00	Significant difference
70	-121.63	-120.56	-134.1624	0.00	Significant difference
80	-121.69	-119.65	-250.9022	0.00	Significant difference
90	-121.53	-120.37	-161.7823	0.00	Significant difference
100	-121.20	-119.76	-180.1282	0.00	Significant difference

Chapter 6

Conclusion

In conclusion, this research presents an alternative approach to traditional RTI by leveraging unintentional EM radiation emitted from computing devices. Unlike conventional RTI systems that rely on complex, symmetric transceiver setups and dedicated hardware, the proposed method offers a simpler, more cost-effective solution suitable for embedded and IoT applications. Experimental results demonstrate that object presence within the LOS causes measurable signal variations, with detectable changes up to 2.4 m indoors and 3 m outdoors. Using a single link signal and EM radiation propagation characteristics, object localization achieved a mean absolute error of 0.1072 m with ability to further improve with tracking techniques such as Kalman filters. To address practical limitations in computational efficiency, a novel weight model algorithm is proposed, offering reduced complexity compared to existing statistical tomography models.

6.1 Contribution

After thoroughly reviewing literature related to tomography and EM side channel analysis, it became evident that no prior work was done combining concepts of tomography and unintentional EM radiations. And the possibility of conducting such research was not presented as a future work in the reviewed papers. Thus ”Leveraging Processor Electromagnetic Radiation for Radio Tomography” is brought forth as a novel

idea.

The main outcomes of the research are as follows,

- Reveal the possibility of utilizing unintentional EM radiation for tomography with evidence for the impact of a human in LOS path.
- Explore possibility of tomography without purpose built transmitters
- Study the propagation characteristics of the unintentional EM radiation
- Propose a new weight model integrating the propagation pattern of a link based on different positions of the object.
- Observe variation of EM side channel from a computing device based on the CPU workload.
- Reveal the security vulnerability with the possibility of detecting movements of people around a desktop computer from a distance.

Additionally, it will contribute to conducting further research in applications of tomography such as object tracking, speed and direction prediction, and activity detection as a novel computer vision technique.

Considering the prior research about profiling a device based on EM emissions, successful result of this research reduces the necessity for transmitters and sensors in close proximity IoT applications. This research will significantly simplify the RTI process and the complexity of wireless sensing networks. The novel setup would eliminate the errors caused by uneven surfaces or faulty transceiver nodes without the requirement for purpose built transmitters.

Radio tomography demands highly efficient sparse reconstruction techniques for fast data processing and to reduce computation cost. Thus, the tomographic imaging model by Wilson and Patwari (Section 5.2) has been improved to make the weight matrix more sparse with results of this research. Further this research exposes a hidden use case of EM side channel and exposes a security threat.

The suggested approach will better suit IoT applications and everyday use, as it is passive and less intrusive than other wireless sensing methods. the use of purpose built transmitters in IoT applications is highly power and space consuming compared to the proposed method. Hence the possible applications of utilizing EM radiation for human detection reduces not only cost but also conserve energy and environment friendly.

6.2 Challenges

- Unavoidable Noise and Multi path Interference

  One of the biggest challenges in this research is environmental noise. This happens when wireless signals reflect off surfaces and take multiple paths before reaching the receiver, sometimes causing unexpected or inconsistent results.

- Limited Resources

  The study was conducted using only one signal source and one receiver. This setup restricted the research to analyzing just a single communication link, limiting the ability to explore broader network behaviors or compare multiple signal paths.

- Requirement of high computing resources

  The data collected during this research amounts to nearly 1 TB, and processing was carried out using a system with 12 GB of RAM. With the available resources, it took approximately 10 minutes to process a single file. This suggests significant potential for efficiency improvements at a larger scale using higher-capacity hardware, which would also be immensely beneficial for real-time processing applications.

6.3 Limitations

The main limitation faced with this research are hardware limitations. The software defined radio had a signal range of 20 MHz which limited the observed frequency range.

Due to lack of resources experiments were conducted with only one signal link. And due to available space and problems of power supply, experiments were conducted in LOS environment.

6.4 Future Work

- Exploring multiple target signals

  This research focuses on utilizing a single frequency band emitted from a desktop device for sensing purposes. However, it was observed that the device emits multiple harmonics with relatively high signal strength, which could also be used for the same purpose.

- Explore generation of EM side channel from computing devices

  Even though it is definite that the signal is coming from the device, how the signal is generated is not fully explained in this research. However, the signal was observed to be sensitive to CPU workload and switch mode power supply. But how side channels are emitted from individual components, what frequency ranges they occupy, and how they might be systematically utilized for sensing can be further studied.

- Device variability and signal selection

  This research is based on a single desktop system. Therefore, it is essential to explore how target signals differ across various devices and to develop a method for identifying and selecting appropriate target signals from different devices.

- Environmental noise and experimental conditions

  The experiments are conducted in an environment filled with inherently ambient noise, including emissions from other elesystematicctronic devices operating nearby. While signal processing assumed relatively constant noise and multipath conditions, an ideal setup for such experiments would involve a controlled environment, such as a Faraday cage or RF-shielded room, to minimize external

interferences.

- Multiple signal sources in the real world

  A real world environment to apply this research would contain multiple electronic devices emitting radiation across a wide range of frequencies. Therefore device fingerprinting methods would need to be accommodate to separately identify devices and then to proceed with capturing target signals.

- Impact of CPU workload on signal strength

  A greater challenge in the real world scenario when targeting computing devices is fluctuating CPU workload. As shown in this research, the signal strength emitted from the device changes with variations in CPU usage. To control this variable during experiments, CPU activity was kept constant using benchmarking tools. However, practical systems must address this challenge before this method can be successfully implemented outside the lab.

- Simplify calibration phase

  The calibration phase plays a critical role in this research. While alternative approaches such as device fingerprinting can reduce or even eliminate the need for calibration, they come with trade-offs—some of which are discussed in Section 2.3.

- Improving accuracy of the tomographic image

  Considering the environmental complexities—including noise, multipath effects, and fluctuating CPU workloads, there is a demand for more accurate and resilient models. Advanced techniques such as improved regularization, adaptive weight models, and particle filters should be explored for use with this concept. Since there is a vast range of radiations emitting from computing devices, one unique approach in this concept would be to utilize multiple signals emitting from the same device to improve accuracy.

- Overcoming Localization Limitations

  The main limitations of this study is the inability to estimate the exact location of

the target object due to the use of a single signal link. This limitation could be addressed by establishing a spatial grid using multiple computing devices and one or more antennas, enabling more accurate localization and tracking. But spatial grid with voxels in the real world will not be symmetrical or even.

Bibliography

Alshami, I., Ahmad, N. & Sahibuddin, S. (2015), 'People's ppresence effect on wlan-based ips' accuracy', *Jurnal Teknologi* **77**, 173–178.

Beetner, D., Seguin, S. & Hubing, T. (2008), 'Electromagnetic emissions stimulation and detection system', *U.S. Patents* .

Bocca, M., Kaltiokallio, O. & Patwari, N. (2013), Radio Tomographic Imaging for Ambient Assisted Living, *in* S. Chessa & S. Knauth, eds, 'Evaluating AAL Systems Through Competitive Benchmarking', Vol. 362, Springer Berlin Heidelberg, Berlin, Heidelberg. Series Title: Communications in Computer and Information Science.

Cui, M., Feng, Y., Wang, Q. & Xiong, J. (2020), Sniffing visible light communication through walls, MobiCom '20, Association for Computing Machinery, New York, NY, USA.

Dharmadasa, M., Gamage, C. & Keppitiyagama, C. (2018), Radio tomographic imaging (rti) and privacy implications, *in* '2018 18th International Conference on Advances in ICT for Emerging Regions (ICTer)', pp. 413–419.

Goldsmith, A. (2005), Path Loss and Shadowing, *in* A. Goldsmith, ed., 'Wireless Communications', Cambridge University Press, Cambridge, pp. 27–63.

Gough, C., Steiner, I. & Saunders, W. (2015), *CPU Power Management*, Apress, Berkeley, CA, pp. 21–70.

Grdović, M. M., Protić, D. D., Antić, V. D. & Jovanović, B. (2022), 'Screen reading: Electromagnetic information leakage from the computer monitor', *Vojnotehnicki glasnik/Military Technical Courier* **70**(4), 836–855.

Guo, Y., Huang, K., Jiang, N., Guo, X. & Wang, G. (2013), An Exponential-Rayleigh signal strength model for device-free localization and tracking with wireless networks, *in* '2013 Fourth International Conference on Intelligent Control and Information Processing (ICICIP)', IEEE, Beijing, China, pp. 108–113.

Hamilton, B. R., Ma, X., Baxley, R. J. & Matechik, S. M. (2014), 'Propagation Modeling for Radio Frequency Tomography in Wireless Networks', *IEEE Journal of Selected Topics in Signal Processing* **8**(1), 55–65.

Hekmat, R. & Mieghem, P. (2006), 'Connectivity in wireless ad-hoc networks with a log-normal radio model', *Mobile Networks and Applications* **11**, 351–360.

Kabir, M. H., Hasan, M. A. & Shin, W. (2022), 'CSI-DeepNet: A Lightweight Deep Convolutional Neural Network Based Hand Gesture Recognition System Using Wi-Fi CSI Signal', *IEEE Access* **10**.

Kaltiokallio, O., Bocca, M. & Patwari, N. (2014), 'A Fade Level-Based Spatial Model for Radio Tomographic Imaging', *IEEE Transactions on Mobile Computing* **13**(6), 1159–1172.

Kaltiokallio, O., Yigitler, H. & Jantti, R. (2014), 'A three-state received signal strength model for device-free localization', *IEEE Transactions on Vehicular Technology* **PP**.

Ke, W., Zuo, H., Chen, M. & Wang, Y. (2019), 'Enhanced Radio Tomographic Imaging Method for Device-Free Localization Using a Gradual-Changing Weight Model', *Progress In Electromagnetics Research M* **82**, 39–48.

Lichtman, M. (2024), 'Frequency Domain — PySDR: A Guide to SDR and DSP using Python'.

Liu, C., Fang, D., Yang, Z., Jiang, H., Chen, X., Wang, W., Xing, T. & Cai, L. (2016), 'Rss distribution-based passive localization and its application in sensor networks', *IEEE Transactions on Wireless Communications* **15**(4), 2883–2895.

Lyons, R. G. (2011), *Understanding digital signal processing*, 3rd ed edn, Prentice Hall, Upper Saddle River, NJ. OCLC: ocn663772861.

Mulder, E. D. (2010), 'Electromagnetic Techniques and Probes for Side-Channel Analysis on Cryptographic Devices', *Katholieke Universiteit Leuven* .

Nath, R. & Tullsen, D. (2017), Chapter 18 - accurately modeling gpgpu frequency scaling with the crisp performance model, *in* H. Sarbazi-Azad, ed., 'Advances in GPU Research and Practice', Emerging Trends in Computer Science and Applied Computing, Morgan Kaufmann, Boston, pp. 471–505.

Niroshan, L., Dharmadasa, I., Edirisinghe, S., Suduwella, C., Sayakkara, A., Keppitiyagama, C. & De Zoysa, K. (2018), Enhancing the Accuracy of Wi-Fi Tomographic Imaging Using a Human-Interference Model, *in* '2018 18th International Conference on Advances in ICT for Emerging Regions (ICTer)', IEEE, Colombo, Sri Lanka, pp. 1–6.

Patwari, N. & Agrawal, P. (2008), Effects of Correlated Shadowing: Connectivity, Localization, and RF Tomography, *in* '2008 International Conference on Information Processing in Sensor Networks (ipsn 2008)', pp. 82–93.

POLIKAR, R. & Lu, B. (1996), 'THE WAVELET TUTORIAL'.

Q Kuisma, M. (2023), 'IQ Data Explained | Amateur Radio – PEØSAT'.

Sasiwat, Y., Jindapetch, N., Buranapanichkit, D. & Booranawong, A. (2019), An experimental study of human movement effects on rssi levels in an indoor wireless network, *in* '2019 12th Biomedical Engineering International Conference (BMEiCON)', pp. 1–5.

Sayakkara, A., Miralles-Pechuán, L., Le-Khac, N.-A. & Scanlon, M. (2020), 'Cutting through the emissions: Feature selection from electromagnetic side-channel data for activity detection', *Forensic Science International: Digital Investigation* **32**, 300927.

Shukri, S. & Kamarudin, L. M. (2017), 'Device free localization technology for human detection and counting with RF sensor networks: A review', *Journal of Network and Computer Applications* **97**.

Signal-to-noise ratio (2024). Page Version ID: 1265000650.

Tarantola, A. (2005), *Inverse Problem Theory and Methods for Model Parameter Estimation*, Vol. xii, SIAM.

Wang, J., Gao, Q., Pan, M., Zhang, X., Yu, Y. & Wang, H. (2016), 'Toward Accurate Device-Free Wireless Localization With a Saddle Surface Model', *IEEE Transactions on Vehicular Technology* **65**(8), 6665–6677.

Wilson, J. & Patwari, N. (2010), 'Radio tomographic imaging with wireless networks', *IEEE Transactions on Mobile Computing* **9**(5), 621–632.

Wilson, J. & Patwari, N. (2011), 'See-Through Walls: Motion Tracking Using Variance-Based Radio Tomography Networks', *IEEE Transactions on Mobile Computing* **10**(5). Number: 5 Conference Name: IEEE Transactions on Mobile Computing.

Wounchoum, P., Vanichpattarakul, T., Dumumpai, K., Chaoboworn, V., Saito, H. & Booranawong, A. (2022), 'Effects of human presence and movement on received signal strength levels in a 2.4 ghz wireless link: An experimental study', *Journal of Electrical Engineering Technology* **17**.

Yang, Z., Qian, K., Wu, C. & Zhang, Y. (2021), *Smart Wireless Sensing: From IoT to AIoT*, Springer International Publishing.

Ye, X., Li, P., Zhao, M., Panda, R. & Hu, J. (2010), 'Scalable Analysis of Mesh-Based Clock Distribution Networks Using Application-Specific Reduced Order Modeling', *IEEE Trans. on CAD of Integrated Circuits and Systems* **29**, 1342–1353.

Yue, Y., Liu, Z., Miao, Y. & Pan, J. (2021), '3D electromagnetic tomography using a single layer sensor array', *Flow Measurement and Instrumentation* **77**, 101850.

Zhao, N., Dublon, G., Gillian, N., Dementyev, A. & Paradiso, J. A. (2015), Emi spy: Harnessing electromagnetic interference for low-cost, rapid prototyping of proxemic interaction, *in* '2015 IEEE 12th International Conference on Wearable and Implantable Body Sensor Networks (BSN)', pp. 1–6.